# EVAULATION OF SPATIAL AND SPATIO-TEMPORAL REGULARIZATION APPROACHES IN INVERSE PROBLEM OF ELECTROCARDIOGRAPHY

A THESIS SUBMITTED TO
THE GRADUATE SCHOOL OF NATURAL AND APPLIED SCIENCES
OF
MIDDLE EAST TECHNICAL UNIVERSITY

BY

MURAT ÖNAL

IN PARTIAL FULFILLMENT OF THE REQUIREMENTS
FOR
THE DEGREE OF MASTER OF SCIENCE
IN
ELECTRICAL AND ELECTRONICS ENGINEERING

SEPTEMBER 2008

Approval of the thesis:

**EVALUATION OF SPATIAL AND SPATIO-TEMPORAL REGULARIZATION APPROACHES IN INVERSE ELECTROCARDIOGRAPHY**

submitted by **MURAT ÖNAL** in partial fulfillment of the requirements for the degree of **Master of Science in Electrical and Electronics Engineering Department, Middle East Technical University** by**,**

Prof. Dr. Canan Özgen _____
Dean, Graduate School of **Natural and Applied Sciences**

Prof. Dr. İsmet Erkmen _____
Head of Department, **Electrical and Electronics Engineering**

Assist. Prof Dr. Yeşim Serinağaoğlu Doğrusöz _____
Supervisor, **Electrical and Electronics Engineering Department**

**Examining Committee Members**

Prof. Dr. Behçet Murat Eyüboğlu _____
Electrical and Electronics Engineering Dept., METU

Prof. Dr. Nevzat Güneri Gençer _____
Electrical and Electronics Engineering Dept., METU

Prof. Dr. Gerhard Wilhelm Weber _____
Institute of Applied Mathematics., METU

Assist. Prof. Dr. Yeşim Serinağaoğlu Doğrusöz _____
Electrical and Electronics Engineering Dept., METU

Dr. Özlem Birgül _____
TÜBİTAK-UZAY

Date: 01/09/2008

**I hereby declare that all information in this document has been obtained and presented in accordance with academic rules and ethical conduct. I also declare that, as required by these rules and conduct, I have fully cited and referenced all material and results that are not original to this work.**

Name, Last name: Murat Önal

Signature:

# ABSTRACT

## EVALUATION OF SPATIAL AND SPATIO-TEMPORAL REGULARIZATION APPROACHES IN INVERSE ELECTROCARDIOGRAPHY

Önal, Murat
M.S., Department of Electrical and Electronics Engineering
Supervisor: Asst. Prof. Dr. Yeşim Serinağaoğlu Doğrusöz

September 2008, 102 pages

Conventional electrocardiography (ECG) is an essential tool for investigating cardiac disorders such as arrhythmias or myocardial infarction. It consists of interpretation of potentials recorded at the body surface that occur due to the electrical activity of the heart. However, electrical signals originated at the heart suffer from attenuation and smoothing within the thorax, therefore ECG signal measured on the body surface lacks some important details. The goal of forward and inverse ECG problems is to recover these lost details by estimating the heart's electrical activity non-invasively from body surface potential measurements. In the forward problem, one calculates the body surface potential distribution (i.e. torso potentials) using an appropriate source model for the equivalent cardiac sources. In the inverse problem of ECG, one estimates cardiac electrical activity based on measured torso potentials and a geometric model of the torso. Due to attenuation and spatial smoothing that occur within the thorax, inverse ECG problem is ill-posed and the forward model matrix is badly conditioned. Thus, small disturbances in the measurements lead to amplified

errors in inverse solutions. It is difficult to solve this problem for effective cardiac imaging due to the ill-posed nature and high dimensionality of the problem. Tikhonov regularization, Truncated Singular Value Decomposition (TSVD) and Bayesian MAP estimation are some of the methods proposed in literature to cope with the ill-posedness of the problem. The most common approach in these methods is to ignore temporal relations of epicardial potentials and to solve the inverse problem at every time instant independently (column sequential approach). This is the fastest and the easiest approach; however, it does not include temporal correlations. The goal of this thesis is to include temporal constraints as well as spatial constraints in solving the inverse ECG problem. For this purpose, two methods are used. In the first method, we solved the augmented problem directly. Alternatively, we solve the problem with column sequential approach after applying temporal whitening. The performance of each method is evaluated.

Keywords: Inverse ECG, Temporal Correlation, Bayesian MAP, Tikhonov Regularization, TSVD.

# ÖZ

## GERİ ELEKTROKARDİOGRAFİ PROBLEMİNDE UZAMSAL VE UZAMSAL-ZAMANSAL DÜZENLİLEŞTİRME YAKLAŞIMLARININ DEĞERLENDİRİLMESİ

Önal, Murat

Yüksek Lisans, Elektrik-Elektronik Mühendisliği Bölümü

Tez Yöneticisi: Yrd. Doç. Dr. Yeşim Serinağaoğlu Doğrusöz

Eylül 2008, 102 sayfa

Geleneksel elektrokardiografi, miyokart enfarktüsü veya aritmi gibi kalp hastalıklarını teşhis etmeye yarayan bir araçtır. EKG, kalpteki elektriksel aktiveden kaynaklanan sinyallerin vücut yüzeyinden ölçülüp değerlendirilmesidir. Ancak, kalbin ürettiği sinyaller vücut içersinde genliklerini kaybedip yumuşamaya maruz kaldıkları için önemli detaylar kaybolur. EKG geri ve ileri probleminde amaç bu kaybolan detayların girişimsiz olarak vucüt yüzeyi potansiyeellerinden kestirilmesidir. İleri EKG probleminde vücut yüzeyi potansiyelleri uygun bir denk kaynak modeli kullanılarak hesaplanır. Geri elektrokardiyografi probleminde amaç, kalbin elektriksel aktivitesini vücut yüzeyinden ölçülen potansiyel değerleri ve gövdenin geometrik modelini temel alarak bulabilmektir. Elektrik sinyallerinin göğüs boşluğunda yumuşama ve zayıflamaya uğramaları nedeniyle geri elektrokardiyografi problemi kötü konumlanmış bir problemdir. Bu nedenle ölçümlerde oluşabilecek küçük değişiklikler çok büyük kestirim hatalarına sebebiyet verir. Kötü konumlanmış

olması ve boyutlarının büyük olmasından dolayı problemin çözülerek etkili kalp görüntüsü elde edilmesi güçtür. Bu sorunları gidermek için çeşitli yöntemler kullanılır. Tikhonov düzenlileştirmesi, TSVD ve Bayes en büyük sonsal (MAP) kestirimi bu metotlara örnektir. En çok kullanılan yaklaşım ise zamansal ilintilerin olmadığı varsayılarak problemin her zaman anında birbirinden bağımsız olarak çözülmesidir (ardaşık sütun yaklaşımı). Bu en hızlı ve en basit yaklaşımdır ancak bu yaklaşım zamansal ilintileri içermez. Bu tezde temel amaç zamansal kısıtların uzamsal kısıtlar gibi EKG geri problem çözüme katılabilmesidir. Bu amaçla, zamansal ilintilerin katıldığı veya katılmadığı farklı düzenlileştirme metotları kullanılmış ve her yöntemin performansları değerlendirilmiştir.

Anahtar kelimeler: EKG Geri problemi, zamansal ilinti, Tikhonov düzenlileştirme, Kısaltılmış Tekil Değerlere Ayrıştırma (TSVD), Bayes en büyük sonsal (MAP) kestirimi

To my family

# ACKNOWLEDGEMENTS

This study was performed under the supervision of Asst. Prof. Dr. Yeşim Serinağaoğlu. I would like to express my sincere appreciation for her support, guidance and insights throughout the study.

This study is part of a project (105E070) that is supported by Turkish Scientific and Technological Research Council (TÜBİTAK). I thank to Dr. Robert S. MacLeod from University of Utah, Nora Eccles Harrison CVRTI and the SCI Institute for the epicardial measurements used in the study and the *map3d* software.

I would like to thank to all my colleagues at MRI research laboratory for their comments and technical supports.

Also, my friends Gül İpek Nakaş, Fatih Nakaş, Ümit Yüksekol, Ali Şengöz, Yeşim Ünsever and Özgün Yılmazok deserve thanks for all their social support and encouragements.

My special thanks go to Irmak Sargın, who owns my heart, for her support and patience during the most stressful times of my life. She keeps me motivated all the time.

Finally, my family, their great support is priceless. I am sure that I would not able to finish this work without their love and affection.

# TABLE OF CONTENTS

# LIST OF TABLE

# LIST OF FIGURES

# CHAPTER 1

## INTRODUCTION

From ancient times, people have been curious about exploring their bodies in order to find cures for their illnesses. After the industrial revolution, new illnesses and disorders were discovered and researchers had started to work on diagnosing these disorders. By improving technologies, clinicians have used different equipments instead of surgical operations for determining the nature of diseases. Electrocardiography (ECG) is one of the most important medical equipments used for investigating the cardiac disorders such as arrhythmia or myocardial infarction. It consists of the interpretation of potentials recorded at the body surface (i.e. torso potentials) due to the electrical activity of the heart [1]. These signals are distorted due to the attenuation and smoothing effects that come from the inhomogeneities within the thorax. Therefore, it is diffucult to estimate the cardiac sources using the surface potentials with a suitable model that relates heart and torso. Mathematically, the cardiac source imaging problem consists of forward and inverse problems. In the forward problem, we calculate the body surface potentials that occur due to equivalent cardiac sources. On the other hand, the estimation of these equivalent cardiac sources from these recorded signals is known as inverse problem of ECG. In this study, we focus on the inverse ECG problem in terms of epicardial potential distribution on the heart surface.

It is difficult to acquire and unite the signals that come from the heart for effective cardiac imaging due to ill-posed nature and high dimensionality of the problem. Many approaches and methods have been proposed to cope with the ill-

posedness of the problem. In this study, we used three essential methods. These are Tikhonov regularization, truncated singular value decomposition (TSVD) and Bayesian maximum a posteriori (MAP) estimation method. In the standard solution approach, we solve the problem at each time instant separately (column sequential method). This is the fastest and easiest method; however, it ignores the temporal information about the problem. Another approach is to solve the problem with temporal correlation assumption. The main aim of this study is to incorporate the temporal correlations into the solution. There are two alternatives to do this; in the first approach, one can solve the entire system in one-step (direct solution). The other approach is to solve the problem after decorrelating it using the assumptions about the structure proposed by Greensite [2]. This allows us to impose spatial and temporal constraints simultaneously. For decorrelation, we applied a smoothing filter to the problem and solved the problem in the transformed domain using the column sequential approach. Then we obtained the desired solution using an inverse transformation.

For testing and comparing these methods, we used three different data sets; two of them are synthetic test data, and the last one includes measured epicardial data from a canine heart. We assessed the performances in terms of relative errors and correlation coefficients. In addition, we examined the 3D visualizations of the results.

## 1.1 Aim of he Study

In this study, we focused on the inverse problem of ECG. The main aim of the study is the evaluation spatial and spatio-temporal regularization approaches that are used for solving the inverse ECG problem. The solution is difficult due to the ill-posed nature of the problem. We use three essential methods for solving this difficulty. However, solution by these methods with the standard column sequential approach does not involve any temporal information. The goal is to apply a procedure to impose the temporal correlation to solution. Another alternative is to solve augmented problem in a complete manner, but this is difficult due to high dimensions of the problem.

## 1.2 Contributions of the Thesis

In this study, we solve the inverse problem of ECG with different methods. The contributions of the can be listed as:

- Methods used in this study were proposed before but not applied to inverse ECG problem with realistic epicardial potentials.
- Derivation of the covariance matrix that will be used in the transformed domain.

## 1.3 Outline of the Thesis

This thesis is composed of seven main chapters and an appendix. Brief contents are given as follows:

Chapter 1 Introduction of the thesis. The objectives and outlines of the study is given in this chapter.

Chapter 2 The background information about ECG and the heart. The previous works on the ECG literature.

Chapter 3 Theory, methods and approaches used in the study.

Chapter 4 Simulation results for comparison of the methods. The results are discussed at the end of this chapter.

Chapter 5 A brief summary, and conclusions. Also, future work that can be carried on will be mentioned.

# CHAPTER 2

## BACKGROUND INFORMATION

The main theme of the thesis is the electrocardiography, especially spatio-temporal regularization of the inverse ECG problem. However, there are several works in literature, such as thesis, books, papers etc. on ECG or the heart in general. These works contain all of the scientific developments starting from the earlier studies on cardiac electricity or physiology. In any case, developments have gone forward by the help of previous works. In this part, we introduce background information related to ECG and the heart.

First, we glance at the literature from a historical perspective. In that part, the most important and breakthrough developments will be given from the beginning of the invention of electricity to recent times.

In the part that follows, we give the anatomy and physiology of the heart. We begin with the heart and its parts. Then, we explain how the heart works from an anatomical point of view. Physiology of the heart from an electrical engineer point of view is another section of this part.

In the third part, we present some examples of recording the electrical activity of the heart. The first one is electrogram, that is obtaining the potential distribution directly from outer and inner surfaces of the heart. The second one is the most

commonly used tool, 12-Lead ECG with its components and contents. The vectorcardiogram and body surface potentials mapping are other examples.

In the last part, we explain how we can estimate the electrical activity of the heart. At the beginning, we introduce the forward and inverse problem of ECG. Then, we give source models that are used in the literature. Especially, we tell the solution procedures that are used in the previous works for epicardial imaging problem.

## 2.1 Historical Perspective

In this part, we present the rich historical background of research on the electrical activity of the heart.

The bioelectric activity has been known for 6000 years. This idea has been proven by an ancient Egyptian hieroglyph of 4000 BC that describes an electric stealthfish (a type of catfish) as a "release of troops". It means that when fishermen caught troops including this type of fish; it gives high voltage electric shock, which resulted in releasing of all fish [3].

The idea of using electromedical equipment for diagnosing and treatment of has been suggested in the 1700s. Neuromuscular stimulation experiments started after the invention of storing electricity by a German inventor Ewald Georg von Kleist (c. 1700-1748) [4]. Galvani performed the most famous of these experiments (Figure 2.1). In his experiment, a frog was lying on the table connected with an electric machine. When the femoral nerve of the frog was stimulated by touching with a small knife, there were sparks in this nearby

electric machine, and muscular contractions occurred in the frog [5]. This phenomenon was proved only after the development of sensitive galvanometer.

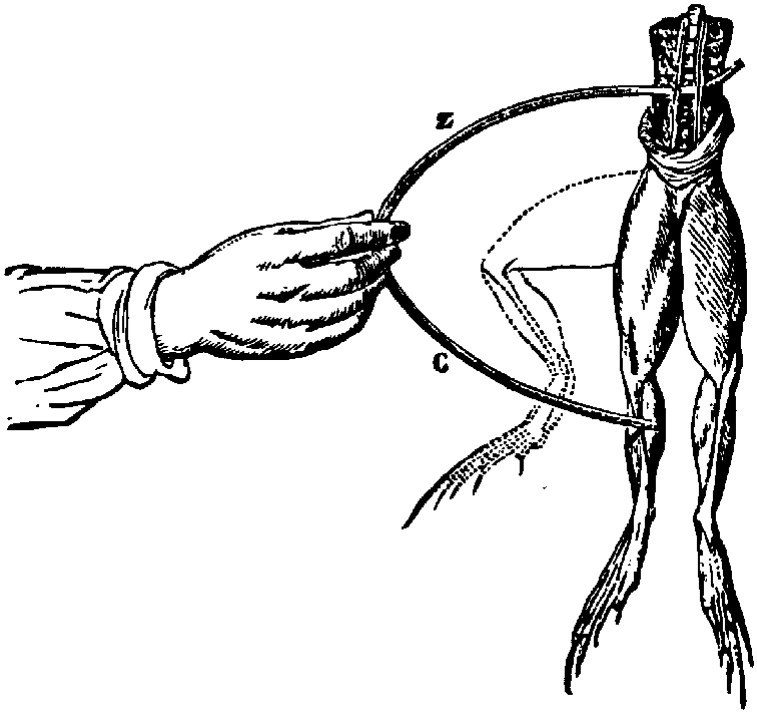


Figure 2.1 : Experiment of Luigi Galvani. Two metal plates [(zinc (Z) and copper (C)], in contact with the electrolytes of tissue produces a current that contracts the frog muscle [6].

Carlo Matteucci is the first person to demonstrate that an electric current is generated for a heartbeat. He also measured resting heart muscle electrical current [7]. Emill DuBois-Raymond has worked on this theme in more detail and explained the relation between changing in electric current and muscle contraction; also, he introduced the term action potential [8]. Augustus Waller is the first person to record the electricity associated with a heartbeat. He recorded the human electrogram using capillary electrometer in 1887 (Figure 2.2) [9]. A French scientist, G.J. Lippman, invented the capillary electrometer in 1876. It contains a glass capillary tube filled with sulphuric acid and mercury, and a moving photographic film. If the potential difference changes, then mercury in

the tube will move. This change in position can be observed by a microscope or projected on a photographic film. The sensitivity of the capillary electrometer was about 1 mV, but its time response was very poor [10].

Waller also suggested that ECG could be recorded using measurements between five points that are formed by the hands, the legs and the mouth.


Figure 2.2 : The first electrocardiogram was recorded by Waller. There are three tracings: (t) is the time marking, (h) is the cardioscope record that shows mechanical movements of apex; (e) the ECG recording by electrometer [6].

The father of modern ECG is Willem Einthoven, a Dutch scientist. He refined Waller's studies by calibrating and correcting the records, he developed the first high quality ECG recorder based on a string galvanometer. In addition, he introduced the simple dipole model of the excitation of the heart. He also published the first ECG lead standard in the literature [11]. He suggested the name for elements of ECG signal that are still in use today (Figure 2.3).

The ECG signal could be amplified after the invention of electron tube. It allowed people to obtain much better recordings. Finally, the invention of transistors opened the electronics era. With technological developments, the

ECG became a user-friendly diagnostic equipment, which can be easily attached to a personal computer.

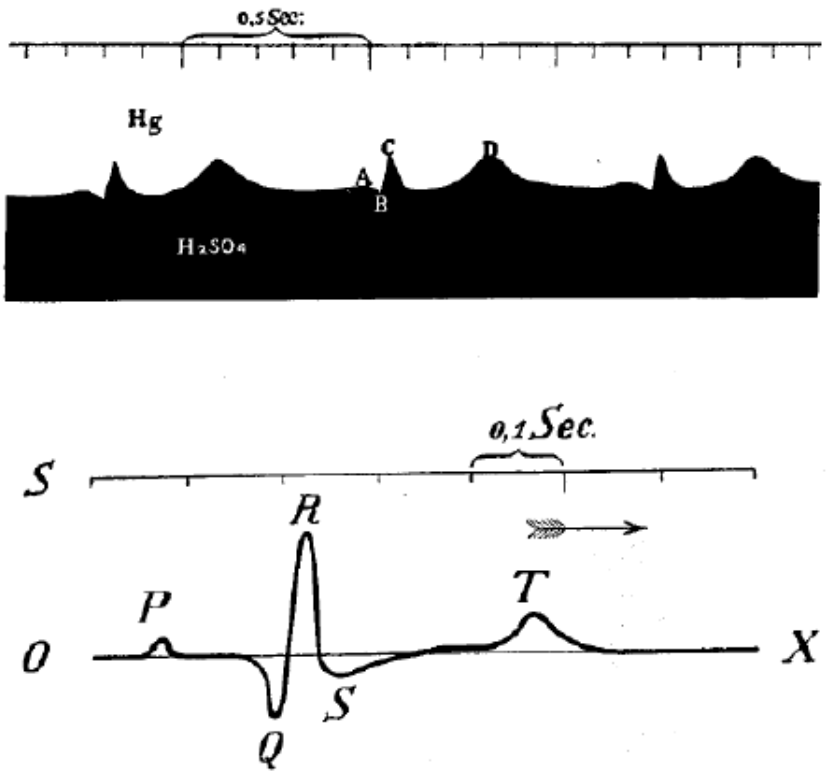


Figure 2.3 : The notation suggested by Einthoven which is similar to that in present [12].

## 2.2 The Heart

The heart is the center of the cardiovascular system. It supplies the blood for feeding and respiration requirements of the body. In this part, we investigate the heart from an anatomical and an electrical point of view. In the first section, we give its biological properties and its working procedure. In the other part, the electrical and mechanical activities of the heart such as contraction of heart

muscle cells and conduction of electric signal in the heart are explained. All materials that are used in this section referenced as [6] [12] [13].

### 2.2.1 Anatomy of the Heart

The heart is located between the lungs in the middle of the chest cavity, behind and slightly to the left of the breastbone (sternum). It is contained in a membrane structure that is called the pericardium. There are four chambers in the heart and various accessory tissues, which are shown in Figure 2.4. Whereas the right part of the heart (right heart) pumps the blood to the lungs for oxygenation, the left part (left heart) pumps blood to the rest of the body. These two parts of the heart are separated by a wall called septum, which prevents any blood flow between the right and left parts of the heart. The circulation path that consists of right heart and lungs is called the pulmonary circulation. The other one is systematic circulation that supplies oxygen and nutrients to the cells of the body.

In the systematic circulation, since the pressure between the arteries and the veins is large, the left part operates as a pressure pump. On the other hand, the pulmonary circulation system has a small pressure difference between the arteries and the veins. Therefore, it is regarded as a volume pump. The left heart is larger and it has a stronger muscle structure in order to supply high pressure levels required for systematic circulation. The volume of blood delivered per unit of time by two sides of the heart is the same when measured over a sufficiently long time.

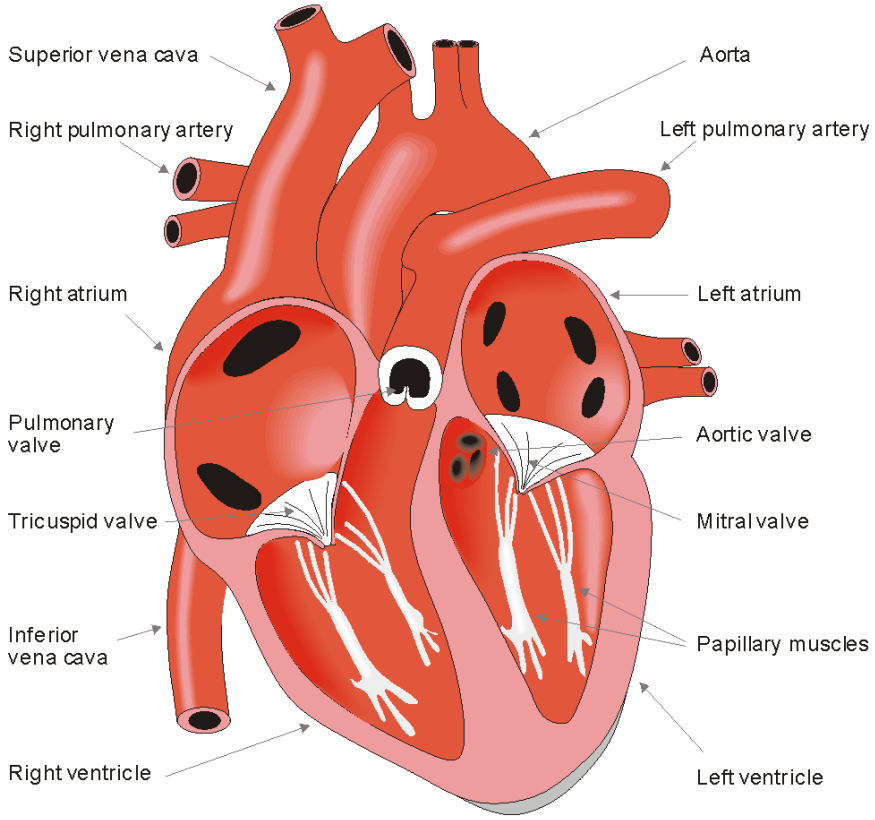


Figure 2.4 : The anatomy of the heart and associated vessels [2].

The chambers of the heart are the right atrium (RA), the left atrium (LA), the right ventricle (RV) and the left ventricle (LV). The walls of the heart are composed of cardiac muscle, called the myocardium. It is situated between the inner surface, i.e., the endocardium, and the outer surface, i.e., the epicardium. The coronary arteries, which surround the left heart, supplies blood required for myocardium. It is a special part of the systematic circulation. The bottom surface of the ventricles is known as the apex, and the upper part of ventricles is called the base.

The heart has four valves. The tricuspid valve lies between the right atrium and the right ventricle, and the mitral valve lies between the left atrium and the left

ventricle. The pulmonary valve lies between the right ventricle and the pulmonary artery, while the aortic valve lies in the outflow tract of the left ventricle (controlling flow to the aorta). The common feature for these valves is that they operate in one way.

The blood returns from the systemic circulation to the right atrium via two main veins, inferior and superior vena cava, and from there goes through the tricuspid valve to the right ventricle. It is ejected from the right ventricle through the pulmonary valve to the lungs. Oxygenated blood returns from the lungs to the left atrium and from there through the mitral valve to the left ventricle. Finally, blood is pumped through the aortic valve to the aorta and from there to the systemic circulation. This cycle is called cardiac cycle.

There are two phases of this cycle, systole and diastole:

- Systole: The ventricles are full of blood and begin to contract. The mitral and tricuspid valves close (between atria and ventricles). Blood is ejected through the pulmonary and aortic valves.
- Diastole: Blood flows into the atria and through the open mitral and tricuspid valves into the ventricles.

### 2.2.2 Electrical Activity of the Heart

In a heart muscle cell, sodium ions flow into the cell based on Hodgkin-Huxley cell membrane model. In this model, the ion pumps and diffusion mechanisms control the flow between the intracellular and extracellular region. The potential

difference between the inside and outside of the cell across the cell membrane is called the transmembrane potential:

$$V_m = \phi_i - \phi_e \tag{2.1}$$

where $V_m$, $\phi_i$, and $\phi_e$, are the transmembrane potential, the intracellular potential and the extracellular potential, respectively. Since the region is quasistatic, we ignore the capacitive, inductive and electromagnetic propagation effects [15].

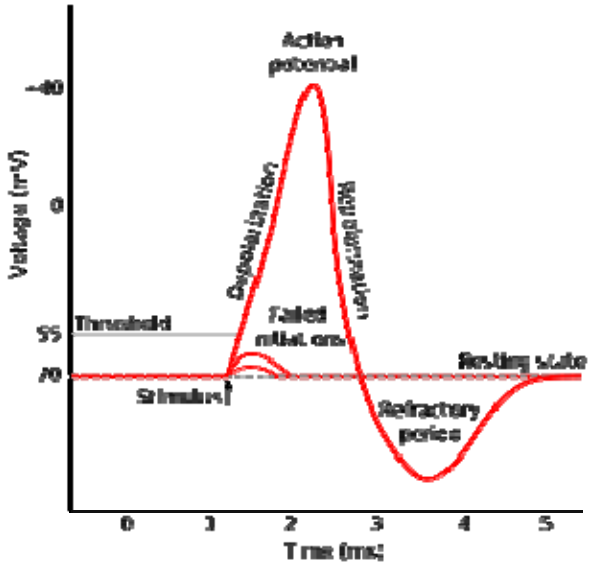


Figure 2.5 : The ideal action potential [16].

After stimulation, changes in the chemical concentrations cause an increase in the transmembrane potential from its resting state to a higher value, then in time it returns back to its resting state. This transmembrane potential is called the action potential (AP) (Figure 2.5). An AP propagates to adjacent cell structure along the path of activation. In the heart muscle, the action potential occurs with

amplitude about 100 mV. A plateau phase follows cardiac depolarization, and thereafter repolarization takes place. Repolarization is a consequence of the outflow of potassium ions. The duration of a typical cardiac AP is about 200-300 ms. This electric signal propagates on the heart.

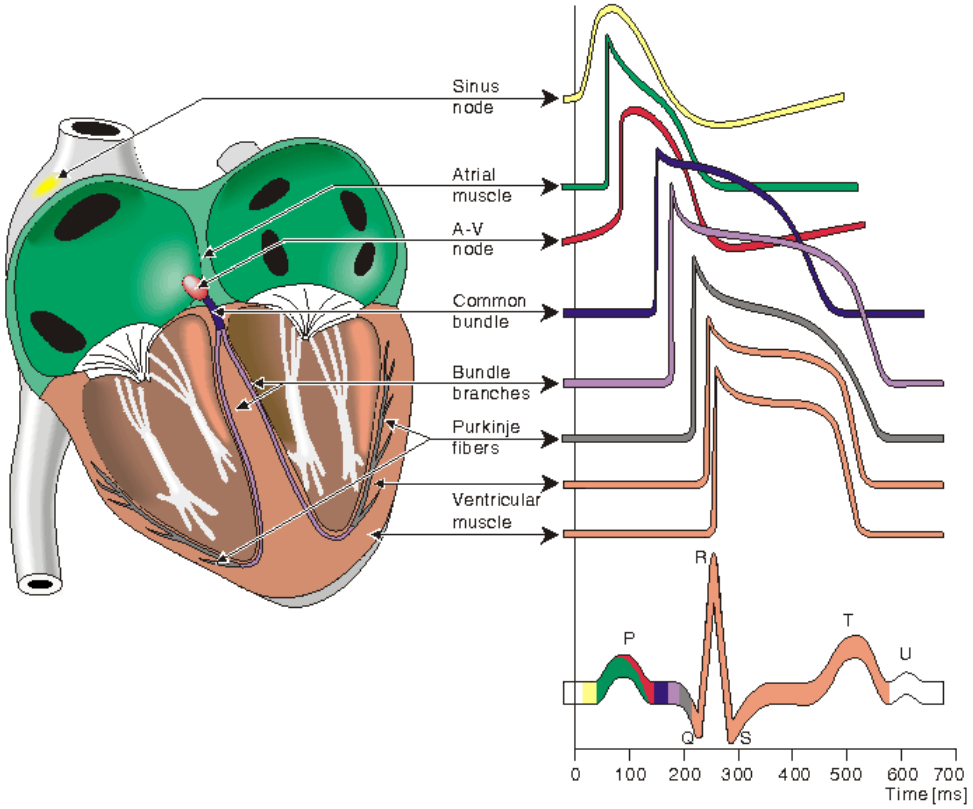


Figure 2.6 : The cardiac conduction system. The propagation of electric signal in the heart and the corresponding waves on the ECG [6].

The sinus node (sinoatrial or SA node), which consists of specialized muscle cells, is located in the right atrium at the superior vena cava. The SA nodal cells are self-excitatory, pacemaker cells. Then impulses spread over and they stimulate the atria and recombine at atrioventricular node (AV) which is located at the boundary between atria and ventricles. Propagation from the AV node to the ventricles is provided by a specialized conduction system. This system is

composed of a common bundle, called the bundle of His. From there, it separates into two bundle branches propagating along the right and left bundle branches, which are called Purkinje fibers that diverge to the inner sides of the ventricular walls. Then ventricles are stimulated. Propagation along the conduction system takes place at a relatively high speed once it is within the ventricular region, but through the AV node, the velocity is extremely slow.

Reflection of this propagating cardiac electric signal onto the body surface is called the electrocardiogram (ECG). A typical ECG signal has P, Q, R, S, T, and U waves (Figure 2.7). P waves represent the atrial depolarization. The shape and duration of the P waves may indicate atrial enlargement. The QRS complex is a structure on the ECG that corresponds to the depolarization of the ventricles. Because the ventricles contain more muscle mass than the atria, the QRS complex is larger than the P wave. The relationship between P waves and QRS complexes helps distinguish various cardiac arrhythmias. In addition, because the His/Purkinje system coordinates the depolarization of the ventricles, the QRS complex tends to look "spiked" rather than rounded due to the increase in conduction velocity. The duration, amplitude, and morphology of the QRS complex is useful in diagnosing cardiac arrhythmias, conduction abnormalities, ventricular hypertrophy, myocardial infarction, electrolyte derangements, and other disease states. The T wave represents the repolarization (or recovery) of the ventricles. The interval from the beginning of the QRS complex to the apex of the T wave is referred to as the absolute refractory period. The last half of the T wave is referred to as the relative refractory period. T waves can be a sign of coronary disorder. The ST interval disorders are the sign of myocardial infarction. The U wave is not always seen. It is typically small, and follows the T wave. U waves are thought to represent repolarization of the Purkinje fibers. An inverted U wave may represent myocardial ischemia or left ventricular volume overload.

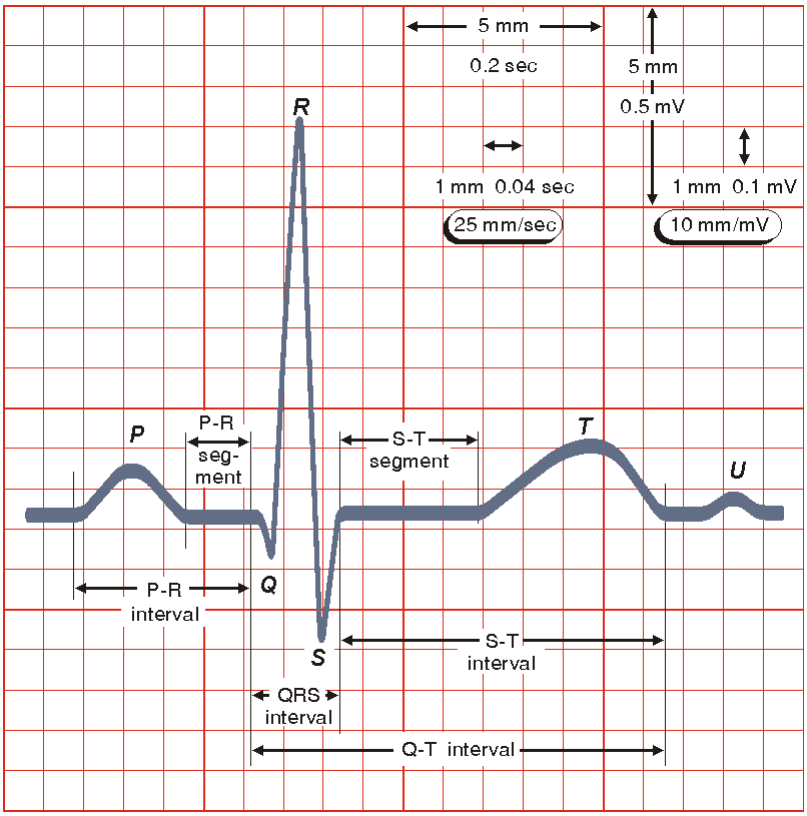


Figure 2.7 : The typical ECG waveform. The waves and intervals are represented [6].

## 2.3 Recording the Electrical Activity of the Heart

In this section, we give some examples about recording and displaying of the electrical activity. Firstly, we define the electrogram, which is a recording of the electrical activity on the epicardium and the endocardium by help of needle electrodes or catheter electrodes. Secondly, we introduce the most known application; 12-lead ECG that is still used in clinical applications. Then, another alternative of ECG, the vectorcardiogram, which is a graphical display of heart activation currents represented by vector loops, is explained. Lastly, we present the body surface potential maps.

### 2.3.1 Electrogram

The term “electrogram” means the record that is the result of change in electric potential. In heart literature, it is used for graphical record that is produced by change in heart electric potential. Especially, this record is obtained by means of electrodes placed directly on the heart tissue instead of on the body surface.

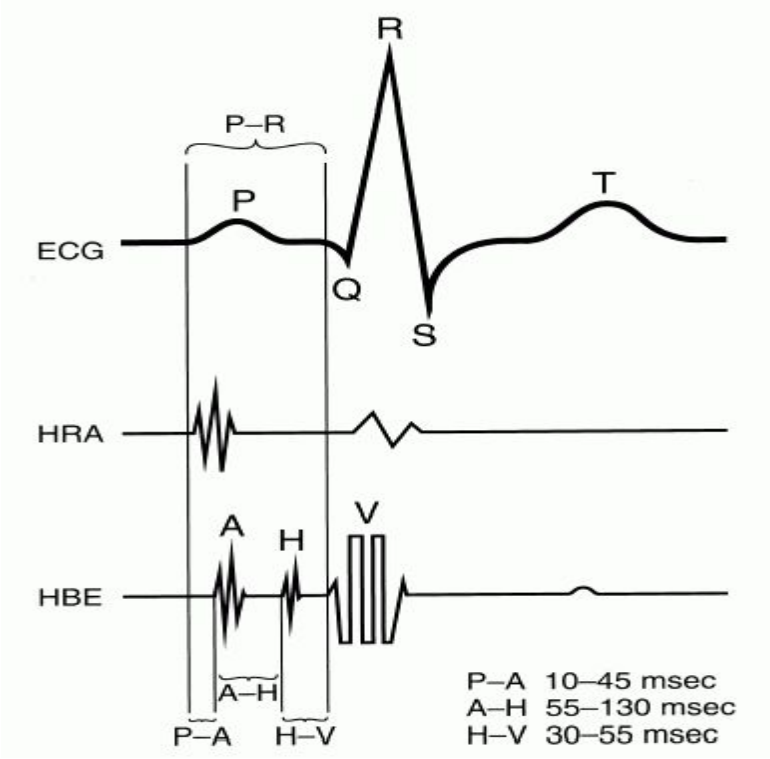


Figure 2.8 : Examples of intracardiac electrograms contrasted with a conventional body-surface electrocardiogram (ECG). HRA = high right atrial electrogram; HBE = His bundle electrogram, in which A = low right atrial activity, H = His bundle activity, and V = ventricular septal activity [17].

The most widely used electrogram in medicine is the His Bundle Electrogram (HBE), which is an intracardiac electrogram of potentials in the lower right

atrium, atrioventricular node, and His-Purkinje system (Figure 2.8). HBE is obtained by positioning intracardiac electrodes near the tricuspid valve [17].

### 2.3.2 12-Lead Electrocardiography

Today for conventional ECG, 12-lead measurements are used. For solution, two-dimensional dipole in the frontal plane in a fixed location is used as equivalent source model and the heart is located in an infinite, homogeneous volume conductor or homogeneous sphere with the dipole in its center (centric dipole model) [2]. Waller recorded the first electrocardiograph using ten leads that were constructed by arms and feet [9]. Einthoven constructed a new lead system [11] that is still in use at present (Figure 2.9).

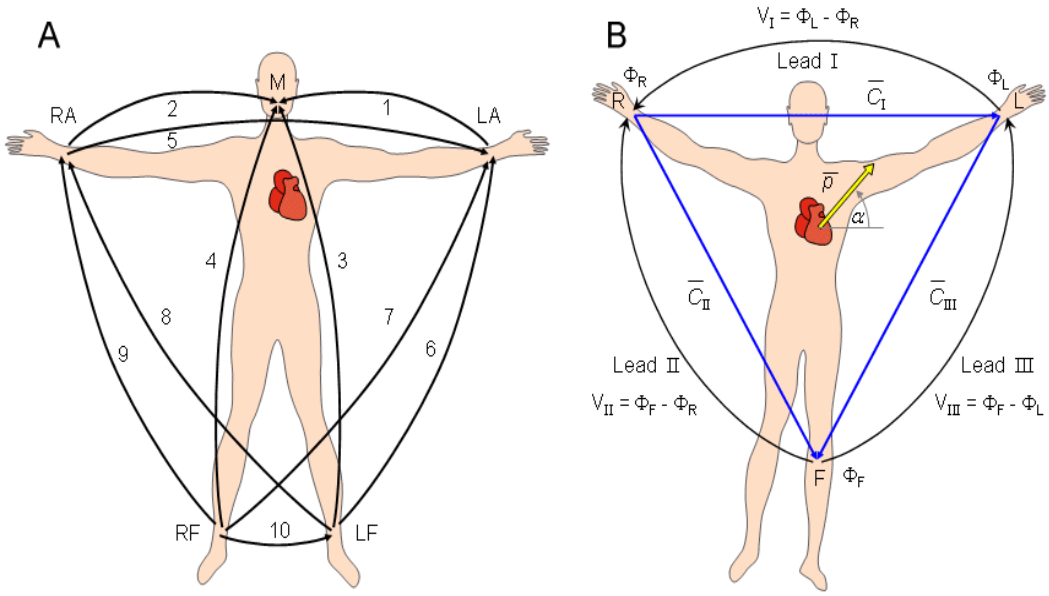


Figure 2.9 : The lead systems that are used for Waller's and Einthoven's recordings and Einthoven triangle and limb leads [6].

The leads that were described by Einthoven are known as the Limb leads. They are derived from various permutations of pair electrodes when one electrode is located on the right arm (R), the left arm (L) and left foot (F):

$$\begin{aligned} &\text{Lead I:} \quad V_I = \Phi_L - \Phi_R \\ &\text{Lead II:} \quad V_{II} = \Phi_F - \Phi_R \\ &\text{Lead III:} \quad V_{III} = \Phi_F - \Phi_L \end{aligned} \tag{2.2}$$

where $V_I$, $V_{II}$, and $V_{III}$ are the voltages of the leads; $\Phi_L$, $\Phi_R$, and $\Phi_F$ are potentials of left arm, right arm and left foot, respectively.

These lead vectors can easily be represented as an equilateral triangle, known as the Einthoven triangle in the frontal plane of the body (the blue triangle in Figure 2.9). From Kirchoff's law, the relationship between the leads is:

$$V_I + V_{III} = V_{II} \tag{2.3}$$

With these assumptions, the voltages measured by the three limb leads are proportional to the projections of the electric heart vector on the sides of the lead vector triangle. Thus, this process allows us to obtain the cardiac vector when we know at least two of three lead vectors.

When we know the cardiac dipole vector $\vec{p}$, the voltage of limb leads can be found using centric dipole model:

Lead I: $V_I = p\cos\alpha$

Lead II: $V_{II} = \frac{1}{2}p\cos\alpha - \frac{\sqrt{3}}{2}p\sin\alpha$ (2.4)

Lead III: $V_{III} = -\frac{1}{2}p\cos\alpha - \frac{\sqrt{3}}{2}p\sin\alpha$

where α is the angle of the cardiac dipole vector

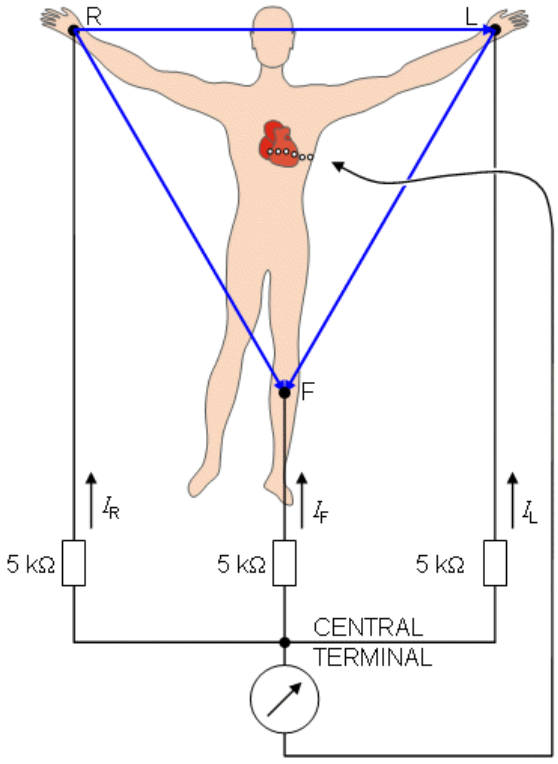


Figure 2.10 : The representation of Wilson central terminal [6].

There are additional three leads in the frontal plane as well as a group of leads in the transverse plane routinely used in clinical ECG. These leads contain measurements of more than one pair of electrode. Thus, they are called the unipolar leads due to potential measurement on one lead with respect to a reference electrode. Ideally, this reference point is infinity. Wilson suggested a central terminal as this reference [18]. He connected a 5kΩ resistor between

each terminal of limb leads to the common point that are call central terminal as shown in Figure 2.10.

From Einthoven triangle, the Wilson central terminal voltage can be found using the Kirchoff's node equation:

$$I_R + I_L + I_F = \frac{\Phi_{CT} - \Phi_R}{5000} + \frac{\Phi_{CT} - \Phi_L}{5000} + \frac{\Phi_{CT} - \Phi_F}{5000} = 0 \tag{2.5}$$

$$\Phi_{CT} = \frac{\Phi_R + \Phi_L + \Phi_F}{3} \tag{2.6}$$

Then, the leads are formed by pairing standard electrode and the Wilson central terminal:

$$\begin{aligned} V_R &= \Phi_R - \Phi_{CT} \\ V_L &= \Phi_L - \Phi_{CT} \\ V_F &= \Phi_F - \Phi_{CT} \end{aligned} \tag{2.7}$$

From the effects of these resistances, the amplitude of the signal observed decreases. They should be modified to augmented limb leads. Goldberger observed that connecting the central terminal to the measurement electrode by omitting the resistance in between supplies improvement on the signal [19]. Then we substitute three unipolar leads with these set of leads, which are known as augmented limb leads (Figure 2.11).

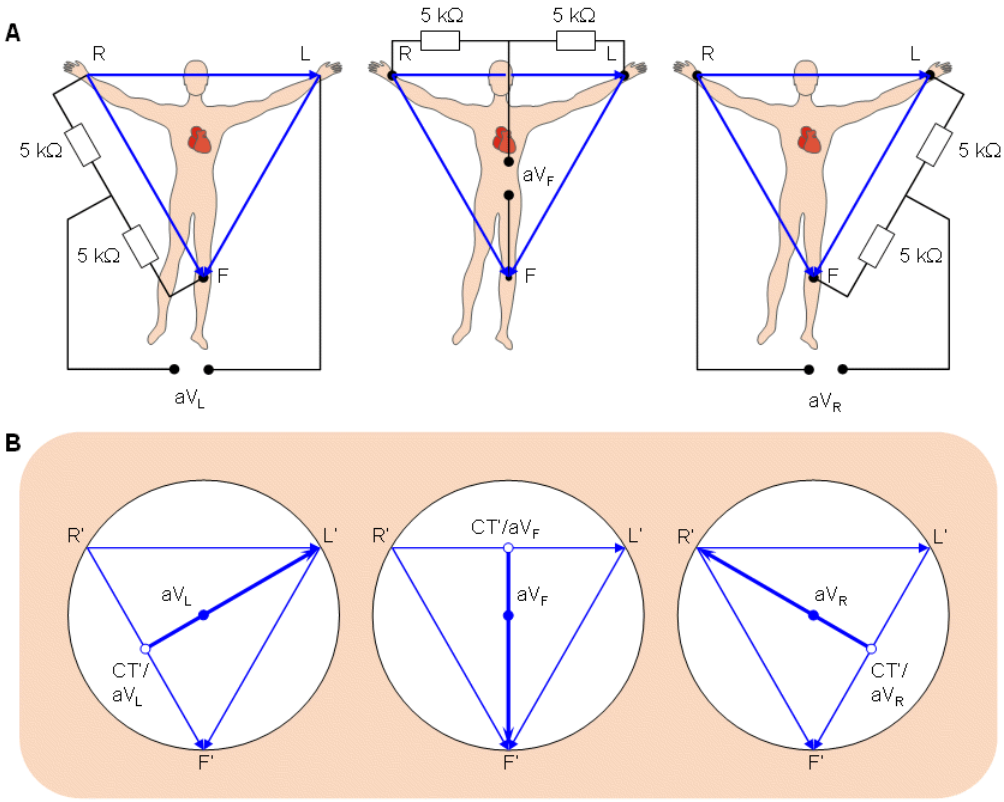


Figure 2.11 : The formation of augmented limb leads and their circuits [6].

We can calculate the voltage of the augmented limb leads from their corresponding circuits:

$$aV_R = \Phi_R - \Phi_{CT/aV_R} = \frac{2\Phi_R - \Phi_F - \Phi_L}{2}$$
$$aV_L = \Phi_L - \Phi_{CT/aV_L} = \frac{2\Phi_L - \Phi_F - \Phi_R}{2} \qquad (2.8)$$
$$aV_F = \Phi_F - \Phi_{CT/aV_F} = \frac{2\Phi_F - \Phi_R - \Phi_L}{2}$$

The augmentation does not affect the direction of the lead vector; it results in increase of the amplitude of the signal.

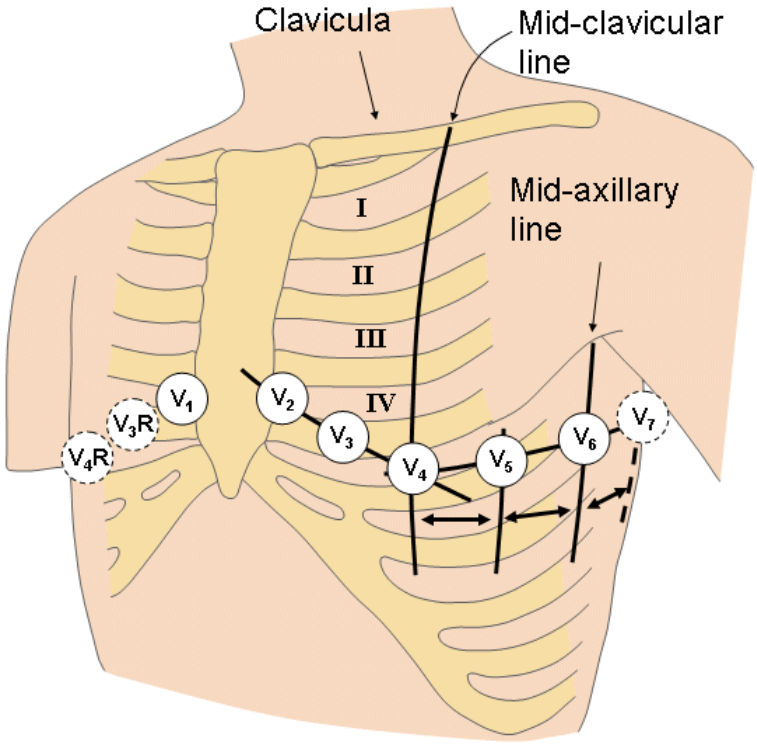


Figure 2.12 : The location of the precordial leads on the chest wall [2].

There are six more leads in the transverse plane in order to measure potentials close to the heart. These leads are called the precordial or chest leads. Wilson introduced these leads in 1944 [20]. These are leads located on the chest wall in a specific position (Figure 2.12).

To summarize, the leads of the 12-lead ECG system are:

- Bipolar Limb Leads (Frontal Plane)
  - Lead I : Right Arm (-) to Left Arm (+); lateral
  - Lead II : Right Arm (-) to Left Foot (+); superior inferior
  - Lead III : Left Arm (-) to Left Foot (+); superior inferior
- Augmented Unipolar Limb Leads (Frontal Plane)
  - Lead $aV_R$: Right Arm (+) to (Left Arm & Left Foot) (-); right forward

- Lead $aV_L$: Left Arm (+) to (Right Arm & Left Foot) (-); left forward
- Lead $aV_F$: Left Foot (+) to (Right Arm & Left Arm) (-); inferior

➢ Unipolar Chest Leads (Transverse Plane)

- Leads V1, V2, V3;
- Leads V4, V5, V6;

### 2.3.3 Vectorcardiogram

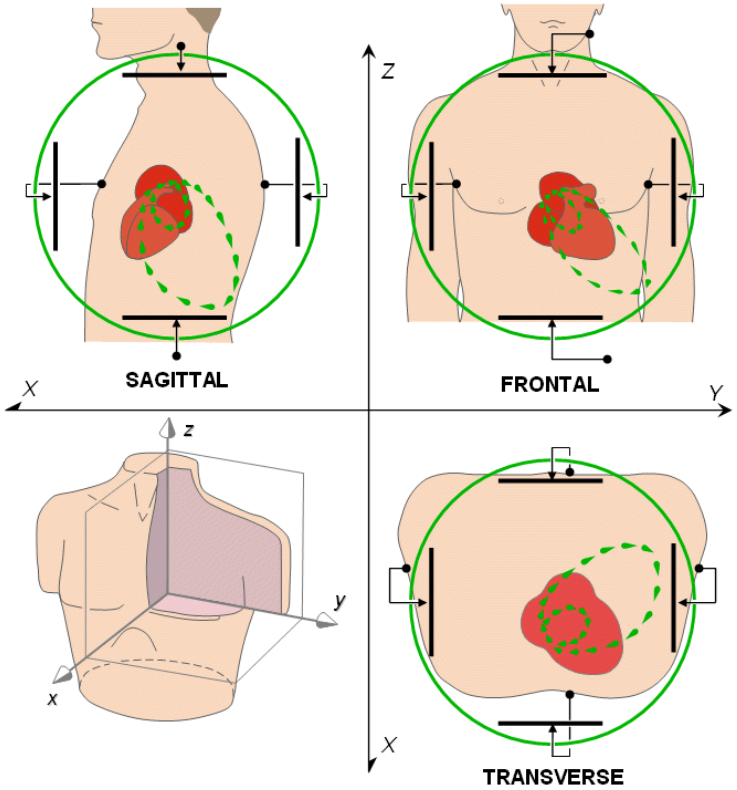


Figure 2.13 : The spatial VCG based on ideal uniform lead fields which are mutually orthogonal being set up by parallel electrodes on opposite sides of the torso (bipolar configuration) [6].

Another alternative to imaging of electrical activity of the heart is the vectorcardiogram (VCG) defined as graphic representation of electrical activity

of the heart with amplitude and direction of the currents. In other words, it is a recording of the three orthogonal components of the electric heart vector. In spatial vectorcardiography (shown in Figure 2.13), we observe the loop that displays the path of the electrical vector on the screen by projecting on to the principle planes. In Figure 2.13, the rectangular coordinate system is a natural selection. These coordinate axes may be either the body axes or the cardiac axes [14].

The signal can be displayed by the three components of the vector as a function of time. It is called the scalar vectorcardiography, but this display is not used very often in VCG, because it does not provide extra information than that obtained from12-lead ECG system.

### 2.3.3 Body Surface Potential Mapping (BSPM)

The last application is the body surface potential mapping. It is defined as recording of body surface potentials to give a complete picture of the effects of the currents from the heart on the body surface. In this technique, the torso potentials are obtained from numerous sites of the thorax using unipolar leads [21]. This may provide more information about the electrical activity of the heart that that of classical ECG. It is usually used for the diagnosis of old inferior myocardial infarction. The disadvantage of this technique is the complexity of the recording and analysis which requires over 100 electrodes and sophisticated equipment since recording these signals at the same time is time consuming and difficult. A typical BSPM examples are shown in Figure 2.14.

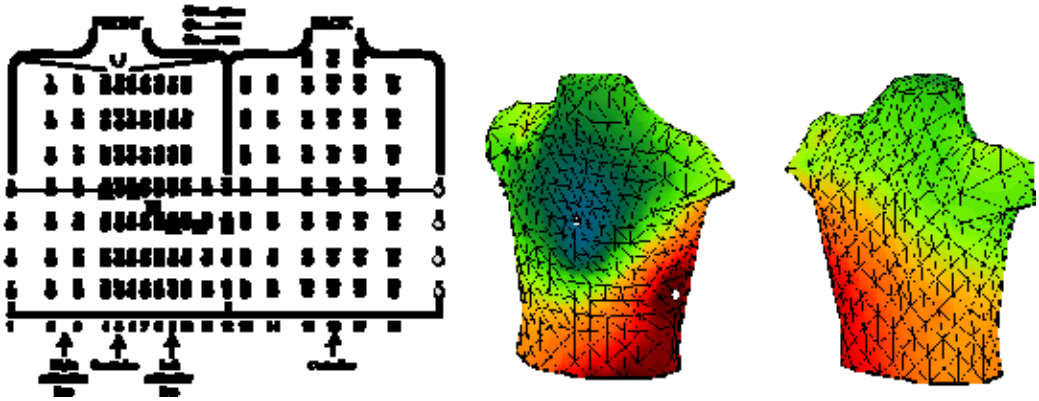

Figure 2.14 : The lead configuration of 128 channel BSPM and its typical result [22].

## 2.4 Estimating the Electrical Activity of the Heart

In this section, we present how one estimates the electrical activity of the heart from body surface potential measurements. The ECG is the tool used for this purpose. As mentioned before, ECG consists of recording of the potentials measured at body surface and the explanation of these records. It is particularly attractive and practical equipment. It is attractive since it is noninvasive therefore surgical operation is not required, and it is practical because the body surface potentials can be easily and rapidly obtained with small numbers of leads using simple electrodes and amplifiers [14].

The electrical activity of the heart can be represented conceptually in terms of an equivalent cardiac electrical source combined with a volume conductor [1]. Estimation of the cardiac sources problem involves forward and inverse problems. The forward problem involves calculating body surface potentials by means of the equivalent source distribution inside the volume conductor, and the inverse problem consists of estimating the source distribution inside the volume conductor by using the measured surface potential distribution. The forward

problem has a unique solution up to a constant for the potential. On the contrary, the inverse problem does not have a mathematically unique solution because the primary cardiac sources cannot be determined uniquely due to inaccessibility of the sources in the active cardiac region for potential measurements [23]. This comes from the fact that the electric field generated by the sources outside the enclosing surface may be duplicated by equivalent sources on the surface [1]. There are many equivalent source models in the literature; therefore, many inverse solutions can be possible. For solving the inverse ECG, firstly, we decide on the equivalent source model and determine its parameters from the body surface potentials using the forward solution.

### 2.4.1 The Forward Problem of ECG

For the forward solution, there are two general approaches: these are surface methods and volume methods. In surface methods, we assume all torso regions are isotropic, thus only the boundaries of different torso regions are taken into consideration in the torso model. Therefore, these methods are also known as boundary element methods (BEM). In the volume methods, we use three-dimensional torso models that are formed by small sub-domain elements. For modeling process, one can use the finite element method (FEM), the finite difference method (FDM) and finite volume methods.

### 2.4.2 The Inverse Problem of ECG

As stated before, the inverse problem does not have a mathematically unique solution because we use a simplified model for the cardiac sources. There are many alternatives for choosing the equivalent source models for cardiac sources such as multipole, moving dipoles, multiple fixed-location dipoles. In addition, the inverse ECG problem can be solved using activation time based models,

epicardial potential distributions or transmembrane potential (TMP) distributions in a three dimensional heart model. The inverse problem has an ill-posed nature that we will investigate in detail in Chapter 3. This ill-posedness results in increase in the number of parameters that are imposed on the desired solution as well as the complexity of the model. Eventually, we have different solutions to the inverse ECG problem depending on the type of the heart model.

#### 2.4.2.1 The Source Models

##### *Multipole Coefficients*

In this model the cardiac sources are represented by infinite series of multipolar sources, at a fixed common location, usually at the center of heart. This idea was first suggested by Arthur [24]. This model is uses the equation:

$$\mathbf{Y} = \mathbf{AX} \tag{2.9}$$

where Y represents the body surface potentials, X represents the multipole coefficients and A is the transfer matrix. The equation is a linear matrix equation with constant coefficients. If the measured potentials are given, then solution can be found by solving a general least-square minimization problem.

$$\mathbf{R} = \left\| \mathbf{Y} - \mathbf{AX} \right\|^2 \tag{2.10}$$

The solution is given as:

$$\hat{\mathbf{X}} = (\mathbf{A}^T\mathbf{A})^{-1}\mathbf{A}^T\mathbf{Y} \tag{2.11}$$

Practically, the solution of (2.10) is easy to solve for few multipole coefficients. The process is repeated for different values of surface potentials during cardiac cycle. However, if we use a homogeneous torso model, we should separate effects of inhomogeneities in the model such as the effects of lungs and blood. The multipole solutions are sometimes used for intermediate step for more complex inverse solutions.

### *Moving Dipoles*

R. M. Arthur conducted experiments to evaluate the moving dipole [25]. In these experiments, he used a finite homogeneous model for the torso. It appeared that the path of the moving electric center of the cardiac activation is within the heart border throughout the cardiac cycle, in the atria during the P-wave and in the ventricles during the QRS- and T-waves.

In this model, cardiac sources are represented by one or two moving current dipoles, which are known as single-moving-dipole (SDM) or two-moving-dipole (TMD). For better estimation, we should select the amplitudes and coordinates correctly. Then, this selection process should be repeated for each time instant. The moving dipole solutions indicate that heart sources consist of one or two localized centers of activity.

The solution can be found by minimizing (2.10) similar to multipole solution. However the problem is no longer linear. Nonlinear iterative methods are used to solve this minimization problem such Levenberg-Marquardt [26].

### *Multiple Dipole Models*

This model was suggested firstly by Fischerman and Barber in 1963 [27] based on a computer model suggested by Selvester [28] consisting of 20 dipoles. In this model, the sources are characterized by a multiple-dipole heart model. The inversely computed dipoles reflect the electric activity of the cardiac regions represented by these dipoles. However, it requires more variables than the other solutions, then obtaining the solution is too difficult, thus there has not been much recent progress. In earlier studies, the solution was obtained from body surface potential maps using the surface Laplacian operator [29].

### *Activation Time Based Models*

During the propagation of the activation wavefront, a large potential difference exists across the moving wavefront that divides the active and inactive tissues [30]. The inverse problem can be modeled in terms of this wavefront [31] [32]. In this model, it is assumed that the field outside the heart is represented as the field produced by a uniform double layer (UDL) of current dipoles along the wavefront in the normal direction. Since UDL is a function of solid angle enclosed by the boundaries of activated regions, one can replace the wavefront by any UDL with the same solid angle. The best choice is the surface lies on the boundary of the heart and enclosed all excited regions. The movement of this surface is modeled using the activation time. With the assumptions constant

voltage step across the wavefront and normal direction of dipole moment, the extracardiac field can be simplified as:

$$\phi_e(y) = \int_{S_v} T(x,y)H(t-\tau(x))dS_x \tag{2.12}$$

where $\phi_e(y)$ is the extracardiac potential at y, H is the Heaviside step function, $\tau(x)$ is the activation time each portion on the cardiac surface ($S_v$), T(y,x) is the transfer function between the point x on cardiac surface and the point y on body surface.

***Epicardial Potentials***

The goal is estimation of epicardial potential distributions from the measured body surface potentials by means of an appropriate torso model. The relation between the torso and epicardium is linear. The formulation consists of this linear relationship and the noise that comes from measurement perturbations and inhomogeneities in the model.

$$Y = AX + N \tag{2.13}$$

In theory, the solution can be found by using (2.11) however, the ill-posedness that comes from the nature of the problem makes it difficult to obtain an effective solution [1]. Therefore, there are many regularization procedures to solve (2.13) such as statistical regularization, Tikhonov regularization, truncated SVD (TSVD), non-linear regularization methods, Bayesian MAP estimation etc.

Tikhonov regularization, TSVD and Bayesian MAP estimation will be explained in detail in the next chapter.

### *Regularization*

Regularization is the method of constraining the solution set using prior information on epicardial potentials. The most widely used regularization method is the Tikhonov regularization [33]. The estimation can be found by solving the minimization problem:

$$\hat{\mathbf{x}}_{\lambda} = \arg \min_{\mathbf{x}} \left[ \left\| \mathbf{y} - \mathbf{A}\mathbf{x} \right\|^2 + \lambda^2 \left\| \mathbf{R}\mathbf{x} \right\|^2 \right] \tag{2.14}$$

The main point is how we can find the optimal regularization parameter, λ. There are several methods proposed in literature to select λ. If the standard deviation of the noise (N in 2.14) is known, it can be found by help of the discrepancy technique [34]. Without requirement of prior information of noise, we can found λ by using techniques such as generalized cross-validation, maximum likelihood estimator [35] [36], and the most commonly used techniques CRESO [37] and L-curve.

In addition, there are many variants of Tikhonov regularization. The most famous one is Twomey's approach [38]. This approach adds a priori estimate, $\mathbf{x}_0$, of epicardial potentials to the second term of the right hand side in (2.14):

$$\hat{\mathbf{x}}_{\lambda} = \arg \min_{\mathbf{x}} \left[ \left\| \mathbf{y} - \mathbf{A}\mathbf{x} \right\|^2 + \lambda^2 \left\| \mathbf{R}(\mathbf{x}\text{-}\mathbf{x}_0) \right\|^2 \right] \tag{2.15}$$

However, the optimality of this solution depends on the correct selection of prior estimation. If it is wrong, the solution is not optimal.

Oster and Rudy [39] have suggested that the components of an epicardial map that have different spatial characteristics can be recovered using different degrees of regularization. They separate the maps using SVD.

Many statistical methods can be applied to epicardial potential imaging. The first statistical approach was proposed by Barr based on Wiener filtering with the use of a covariance matrix for characterization of epicardial potentials [40].

### *Imposing Temporal Information*

The methods described in the previous part do not necessarily contain any temporal information about the epicardial potentials. We know that there is correlation between potential values of different nodes for different time instants. Therefore, we need to impose some temporal constraints on the epicardial potentials. Oster and Rudy [41] suggested using Twomey regularization to impose the temporal constraints. They used different prior estimates for Twomey regularization such as combination of previous and forward potential values. For example:

$$X_0 = 2X_{j-1} - X_{j-2} \tag{2.16}$$

Here ‘j-1’ and ‘j-2’ represent the time instants before the current time ‘j’. He tested his suggestion with an isolated canine heart experiment conducted using an isolated dog heart located in a metal tank filled with an electrolytic solution.

Brooks et al. [42-44] suggested a second approach. He proposed adding another constraint to (2.15) that incorporates the temporal dynamics of the epicardial potentials:

$$\hat{\mathbf{x}}_{\lambda} = \arg \min_{\mathbf{x}} \left[ \left\| \mathbf{y} - \mathbf{A}\mathbf{x} \right\|^2 + \lambda^2 \left\| \mathbf{R}\mathbf{x} \right\|^2 + \eta^2 \left\| \mathbf{T}\mathbf{x} \right\|^2 \right] \tag{2.17}$$

Whereas **R** is the Tikhonov spatial regularization matrix, **T** is the temporal regularization matrix. Then the solution can be obtained as:

$$\hat{\mathbf{x}} = (\mathbf{A}^T\mathbf{A} + \lambda^2\mathbf{R}^T\mathbf{R} + \eta^2\mathbf{T}^T\mathbf{T})^{-1}\mathbf{A}^T\mathbf{y} \tag{2.18}$$

He used a vector notation for describing the formulation. Then he used Kronecker product for the block matrix notation. Thus, the problem has high dimensions. He describes two algorithms for solving this high dimensional problem. First algorithm is block Jacobi method and the other one uses Kronecker product decomposition.

Greensite proposes another method [2] [45]. He suggested several possible statistical assumptions on the unknown matrix **X,** such that $C_X$ is simplified and completely and partially estimated from the measurements. This method will be explained in Chapter 3 in details.

The last method for imposing temporal constraints using Kalman filtering. Kalman filtering was firstly used for inverse problem especially in inverse ECG by a group in Finland [46-47]. In the method, first the state-space model of the problem is obtained:

$$\mathbf{x}_{k+1} = \mathbf{F}\,\mathbf{x}_k + \mathbf{w}_k \tag{2.19}$$

$$\mathbf{y}_{k+1} = \mathbf{H}\,\mathbf{x}_{k+1} + \mathbf{v}_{k+1} \tag{2.20}$$

where x, y represent epicardial and body surface potentials, respectively, F is the state transition matrix and H is the forward transfer matrix, w and u are the state and measurement noise vectors.

The state transition matrix F contains the temporal information of the unknowns at two neighboring time instants. Decomposing the covariance matrix, $C_X$, the solution can be found by applying Gauss elimination followed by block back substitution that can be realized by Rauch-Tung-Striebel (RTS) algorithm [48]:

$$(\sigma_{\mathbf{n}}^2\mathbf{C}_{\mathbf{x}}^{-1} + \mathbf{A}^T\mathbf{A})(\mathbf{x} - \overline{\mathbf{x}}) = \mathbf{A}^T(\mathbf{y} - \overline{\mathbf{y}}) \tag{2.21}$$

## 2.5 Summary

In this chapter, we have given background information about the electrocardiography, especially the inverse ECG. First, we summarized the rich past of research on cardiac electrophysiology and ECG. Then we described the

anatomy and physiology of the heart. Next, we gave some brief information about ECG and its applications. Finally, we explained the methods in literature that can be used for solving the inverse ECG problem.

# CHAPTER 3

## THEORY

In this section, the theory and the methods used in this dissertation will be presented. As mentioned before, we can define inverse problem of ECG as estimation of the electrical activity of the heart using body surface measurements and a suitable mathematical model of the torso. In the inverse problem, one cannot obtain a mathematically unique solution because the cardiac sources cannot be determined uniquely. Therefore, it is possible to use different equivalent source types for modeling the cardiac sources. We assume all the sources on the epicardium. In addition, the problem is ill-posed due tot nature of the problem and the forward solution matrix is ill-conditioned. Therefore, one should apply a procedure called the regularization to the problem prevent the large errors in the solution.

The regularization process can be defined as adding additional information about the desired solution into the problem in order to stabilize the problem. In inverse problem literature, there are different regularization methods such as Tikhonov regularization, truncated singular value decomposition (TSVD), statistical regularization, constrained least square regularization, nonlinear regularization methods or augmented source formulation etc. In this study, we have used three of them. These are Tikhonov regularization, TSVD and Bayesian maximum a posteriori (MAP) estimation.

In this study, we use two different approaches. These are column sequential approach and the solution of the problem with regard to temporal relations. In the first one, one solves the problem traditionally for each time instant independent with the assumption that there is no correlation between the time instants. On the other hand, in the temporal correlation assumption, one can use two alternatives to solve the problem: 1) The direct solution - we solve the augmented problem that is created by combining the linear equations at each time instant end to end. 2) Temporal whitening - we decorrelate the system and then we apply the column sequential approach to the problem with some appropriate statistical assumptions. Furthermore, during the application of the Bayesian MAP estimation, we can use separability condition, which states that covariance matrix of the unknown can be represented in terms of temporal and spatial covariance matrices.

In the first section, we explain the problems and its properties. In the next section, we will present the essentials methods and approaches that are used in this study. In this section, we will give the definition and derivation of the methods.

### 3.1 Problem Definition and Characteristics

In the forward solution of ECG, one computes the potential distribution on the body surface due to equivalent electrical sources in the heart. When the equivalent sources in the heart are epicardial potentials, the forward solution indicates a linear relationship between body surface potentials and the epicardial potentials:

$$\mathbf{Y} = \mathbf{AX} + \mathbf{N} \tag{3.1}$$

In this formulation, $\mathbf{Y} \in R^{p \times t}$ represents the known matrix, the measurements on the body surface; $\mathbf{X} \in R^{m \times t}$ represents the unknown matrix, the epicardial potentials. $\mathbf{A} \in R^{p \times m}$ is the transfer matrix that is obtained by forward solution of the problem. Also, $\mathbf{N} \in R^{p \times t}$ is the noise in the measurements. Each column represents the time instant. Each row of **X** is the node on the heart, each row of **Y** and **N** is the node on the torso.

We can also represent the problem in an augmented way:

$$\begin{bmatrix} \mathbf{Y}_{:1} \\ \vdots \\ \mathbf{Y}_{:t} \end{bmatrix} = \begin{bmatrix} \mathbf{A} & & 0 \\ & \ddots & \\ 0 & & \mathbf{A} \end{bmatrix} . \begin{bmatrix} \mathbf{X}_{:1} \\ \vdots \\ \mathbf{X}_{:t} \end{bmatrix} + \begin{bmatrix} \mathbf{N}_{:1} \\ \\ \mathbf{N}_{:t} \end{bmatrix} \tag{3.2}$$

Alternatively, (3.1) and (3.2) can be written for each time instant separately:

$$\mathbf{Y}_{:i} = \mathbf{AX}_{:i} + \mathbf{N}_{:i} \qquad \text{i=1,2,....,t} \tag{3.3}$$

The problem is ill-posed due to the discretization and attenuation effects in the mathematical model, i.e. small variations on the measurements or small imperfections on the forward model causes unacceptable errors in the solution [49]. The concept of ill-posedness is depicted firstly by Jacques Hadamard in the first quarter of the twentieth century. He has defined the term "ill-posed" as if the system has not a unique solution or has not a continuous function of the data.

Also, he concluded that ill-posed problems cannot be used for representations of the physical systems. Today, we know that his thought was mistaken and many physical systems are represented using inverse problems [50].

In the formulation, **A** is an ill-conditioned matrix due to the ill-posedness of the problem. An ill-conditioned matrix has very large condition number, which means that some of the equations of the systems are mathematically linearly dependent [51]. This may result in incorrect mathematical modeling of the system, thus it should be arranged in a correct way before computing the numerical solution in order to decrease the error.

### 3.2 Solution Strategies

The illposedness of the inverse problem can be removed using a procedure called the regularization—imposing a priori constraint to the problem supplies smaller solution sets such that some of the unstable solutions are thrown out from the solution set [51].

There are various regularization techniques such as Tikhonov regularization, statistical regularization, and nonlinear methods. The most popular direct regularization method is Tikhonov regularization that is regarded as adding constraints to the typical least square minimization problem [33] [52]. TSVD is a type of singular value decomposition (SVD) such that one calculates the decomposition approximately by cutting of the process at a convenient step [51]. Another alternative is the Bayesian MAP estimation in which one maximizes the a posteriori probability density function (pdf) assuming that the prior pdf of the parameter is known [53]. Also, one can use constrained least-square that is a

modified type of Tikhonov regularization. In this method, the preliminary estimate is adding to constraints [41]. In addition, nonlinear regularization techniques can be applied. An example provided in [54].

We use three essential methods for obtaining the solution; these are Tikhonov Regularization, Truncated Singular Value Decomposition (TSVD) and Bayesian Maximum A posteriori (MAP) Solution. The approaches that are followed for the solution can be classified in terms of adding the temporal behavior of the system or not.

The traditional approach for the solving the inverse ECG problem is the column sequential method, which it is assumed that there is no correlation between the epicardial potentials at different time instants. This method is easy and fast, but it ignores temporal dynamics of the problem. One can use two approaches to add the temporal dynamics to the solution. The first one is the direct solution with adding temporal dynamics. In this method, we solve the augmented problem in (3.2), but this approach yields a computational complexity. An alternative to direct solution is temporal whitening. In this method, first, an orthogonal transformation is applied to the equation system, and then the problem is solved in that domain using the column sequential approach, finally the solution is transformed back to its original domain [2]. In Bayesian solution, we can use separability condition [44]. It is not a solution procedure; however, it gives a chance to model temporal and spatial dynamics of the problem separately.

In this section, we have briefly explained the regularization methods and approaches that are used in this study. The detailed information will be given in the next sections. For the following section, derivations of the methods are calculated for the problem:

$$\mathbf{y} = \mathbf{A}\mathbf{x} + \mathbf{n} \tag{3.4}$$

where $\mathbf{A} \in R^{p \times m}$ , $\mathbf{x} \in R^{m \times 1}$ , $\mathbf{y} \in R^{p \times 1}$, $\mathbf{n} \in R^{p \times 1}$

### 3.2.1 Tikhonov Regularization

In this section, we investigate Tikhonov regularization method and its components. It is the most popular numerical treatment of discrete ill-posed problems. The method has been developed by A. N. Tikhonov in 1977 [33].

In the method, one adds a term to the least square equation in order to limit the solution space depending on the constraint that is represented by this term. In other words, the solution set of the problem is narrowed such that the number of unstable solutions in the set reduce. However, as a price to be paid, the resolution reduces and the estimation is unbiased.

The general form of the Tikhonov regularization leads to a least square minimization problem:

$$\hat{\mathbf{x}}_{\lambda} = \arg \min_{\mathbf{x}} \left[ \left\| \mathbf{y} - \mathbf{A}\mathbf{x} \right\|^2 + \lambda^2 \left\| \mathbf{R}\mathbf{x} \right\|^2 \right] \tag{3.5}$$

where R is the regularization matrix which defines the constraints. It can be chosen as identity matrix for the zero order Tikhonov regularization. (R=G, surface gradient operator for the first order Tikhonov regularization, and R=L, the surface Laplacian operator for the second order Tikhonov regularization). On

the other hand, λ is the regularization parameter that controls the relationship between increase in stability and decrease in the resolution of the problem.

There are two different representation forms for Tikhonov regularization:

$$(\mathbf{A}^T\mathbf{A} + \lambda^2\mathbf{R}^T\mathbf{R})\mathbf{x} = \mathbf{A}^T\mathbf{y} \tag{3.6}$$

$$\hat{\mathbf{x}}_\lambda = \arg\min_{\mathbf{x}} \left[ \begin{pmatrix} \mathbf{A} \\ \lambda\mathbf{R} \end{pmatrix} \mathbf{x} - \begin{pmatrix} \mathbf{y} \\ 0 \end{pmatrix} \right] \tag{3.7}$$

It can be seen from the formulation that if the null spaces of the A and R intersect trivially such that the coefficient matrix has full rank, then the solution is unique. The explicit equation for the regularized solution is given by:

$$\mathbf{x}_\lambda = (\mathbf{A}^T\mathbf{A} + \lambda^2\mathbf{R}^T\mathbf{R})^{-1}\mathbf{A}^T\mathbf{y} \tag{3.8}$$

The regularization parameter, λ is chosen by using different techniques such as L-curve [51], CRESO [37] or minimum RE condition.

L-curve is the most suitable graphical tool for comparing the seminorm of the regularized solution and the corresponding residual norm. It is a continuous curve if the parameters are continuous as in Tikhonov regularization. On the contrary, for discrete parameters such as in TSVD the curve contains discrete points. It has an L-shaped appearance and a distinct corner separating vertical

and horizontal parts of the curve. Figure 3.1 shows a typical L-curve for Tikhonov regularization obtained from the epicardial data.

L- curve shows the possibility of choice of our parameters. Any choice of parameter under the curve does not give any solution. The value at the corner of the plot is best choice for the regularization.

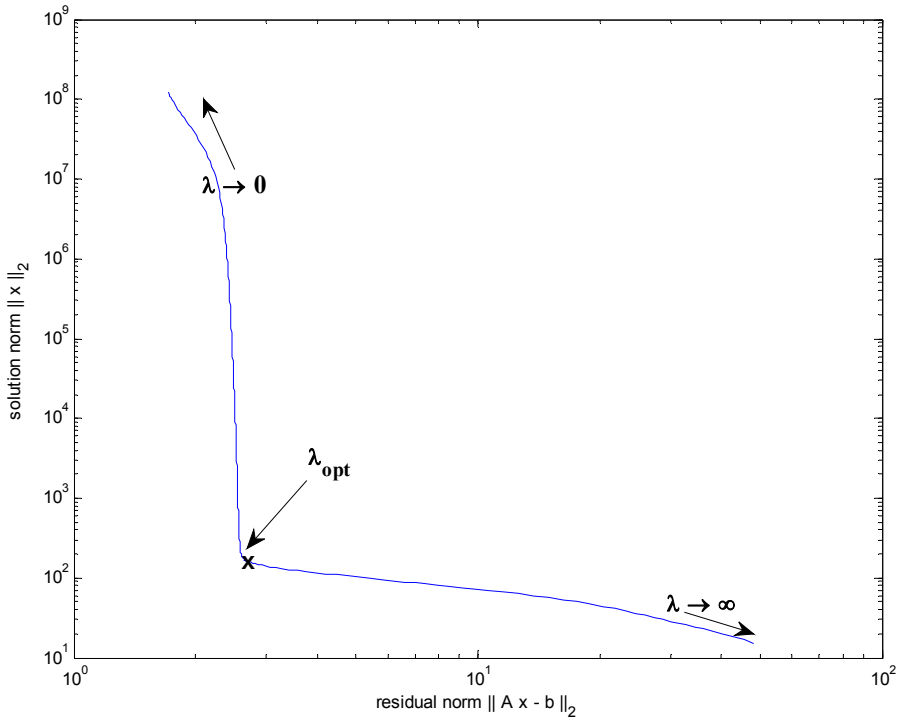


Figure 3.1 : The typical L- curve for Tikhonov regularization

Another method to choose regularization parameter is Composite Residual and Smooth Operator (CRESO) technique. This method estimates the regularization parameter using measured data and geometry without requiring the information about the type of errors or upper bound of measurements [37]. The parameter can be found as the positive smallest λ among those that maximize the function C(λ):

$$C(\lambda) = \|\mathbf{L}x\|^2 + 2\lambda \frac{d}{d\lambda}\|\mathbf{L}x\|^2 \tag{3.9}$$

Another alternative method is minimum relative error method. We can apply this technique for the simulation studies in which the true solution of the problem is known. In this technique, we chose λ values from an interval. Each $\lambda_i$ value within our pre-selected interval is substituted in equation (3.5) and the corresponding relative error is computed:

$$\mathrm{RE} = \sqrt{\frac{\sum_{i=1}^{t} \left\| \mathbf{x} - \hat{\mathbf{x}}_{\lambda_i} \right\|^2}{\sum_{i=1}^{t} \|\mathbf{x}\|^2}} \tag{3.10}$$

where, **x** represents the true solution and $\hat{\mathbf{x}}_{\lambda_i}$ shows the estimation of **x**. The regularization parameter is chosen as $\lambda_i$ value that gives the minimum RE value.

### 3.2.2 Truncated Singular Value Decomposition (TSVD)

Truncated SVD is a type of singular value decomposition that is defined as cutting decomposition process in a suitable step and calculating the approximated result. It is more efficient than normal decomposition since truncation process allow us to throw small singular values from the decomposition. First, we define the SVD and we explain how we can truncate the procedure and obtain TSVD [51].

For a rectangular matrix $\mathbf{A} \in R^{p \times t}$ and $p \geq t$, the singular value decomposition can be found by the formula:

$$\mathbf{A} = \mathbf{U}\boldsymbol{\Sigma}\mathbf{V}^{T} = \sum_{i=1}^{t} u_i \sigma_i v_i^{T} \tag{3.11}$$

where $\mathbf{U} = (u_1, ..., u_t)$ and $\mathbf{V} = (v_1, ..., v_t)$ are unitary matrices with orthonormal columns $\mathbf{U^T U} = \mathbf{V V^T} = \mathbf{I}_t$; $\Sigma = (\sigma_1, ..., \sigma_t)$ is a diagonal matrix whose diagonal entries are nonnegative elements that are sorted in a nonincreasing order ($\sigma_1 \geq ... \geq \sigma_t$). $\sigma_i$ are called the singular values of the matrix **A**; $u_i$ and $v_i$ are the right and left singular vectors respectively. For any dimensions p<t, we apply SVD to the $\mathbf{A}^T$ instead of **A**, then **U** and **V** interchange. The inverse matrix of A can be computed by using SVD as:

$$\mathbf{A}^{-1} = \sum_{i=1}^{r} u_i \frac{1}{\sigma_i} v_i^{T} \tag{3.12}$$

Therefore, if there are smaller singular values, the inversion diverges due to the $1/\sigma_i$ term. This means that the smaller perturbations in the small singular values result in amplified error in the solution. Hence, some of the singular values are dropped in the sum in order to handle this difficulty.

In TSVD, the decomposition process in equation (3.11) is truncated at $k^{th}$ step, only the biggest "k" singular values are calculated and remaining ones are thrown out. Also, **U** and **V** matrices are calculated until the $k^{th}$ step,

$\mathbf{U} = (u_1, ..., u_k)$ , $\mathbf{V} = (v_1, ..., v_k)$. Thus, the process is accelerated and the error is decreased.

The TSVD for the matrix **A** is computed using this formula:

$$\tilde{\mathbf{A}}_k = \sum_{i=1}^{k} \mathrm{u_i} \sigma_\mathrm{i} v_\mathrm{i}^\mathrm{T} \qquad \mathrm{k} \le \mathrm{t} \tag{3.13}$$

Expectedly, the TSVD is not an exact decomposition of the matrix; it is only an approximation of its SVD. In other words, $\tilde{\mathbf{A}}_\mathrm{k}$ is the closest approximation of **A** of which rank is k. The solution is obtained using the TSVD is given by:

$$\hat{x}_k = \mathbf{A}_k^{-1} y \quad \Rightarrow \quad \hat{x}_k = \sum_{i=1}^{k} \mathrm{v_i} \frac{1}{\sigma_\mathrm{i}} u_\mathrm{i}^\mathrm{T} y \tag{3.14}$$

### 3.2.3 Bayesian Maximum A Posteriori (MAP) Estimation

The last essential method is Bayesian MAP estimation. In Bayesian philosophy, one estimates the posterior probability distribution of the unknowns with known prior probability density function (pdf). This prior distribution may help impose the user's subjective judgment, or it may incorporate information from other experiments [55].

In the model, **x** and **y** are assumed to be random with joint pdf p(**y,x**) and p(**x**) is the known prior pdf of unknown **x**. p(**y**) is the marginal pdf of the measurements

and p(**y****x**) is the conditional probability of measurements onto unknown **x**. p(**x****y**) is the posterior pdf, that refers to the pdf of **x** after data is observed. We begin with Bayes' theorem:

$$p(\mathbf{x} \setminus \mathbf{y}) = \frac{p(\mathbf{y} \setminus \mathbf{x})\, p(\mathbf{x})}{p(\mathbf{y})} \tag{3.15}$$

One can write from the definition condition probability by help of Bayes' theorem:

$$p(\mathbf{y}, \mathbf{x}) = p(\mathbf{x} \setminus \mathbf{y})\, p(\mathbf{y}) = p(\mathbf{y} \setminus \mathbf{x})\, p(\mathbf{x}) \tag{3.16}$$

Also, the marginal pdf of the measurement, **y** can be written as:

$$p(\mathbf{y}) = \int p(\mathbf{y}, \mathbf{x}) d\mathbf{x} \tag{3.17}$$

When (3.16) and (3.17) are substituted in (3.15); the posterior pdf that is estimated for **x** given **y** becomes:

$$p(\mathbf{x} \setminus \mathbf{y}) = \frac{p(\mathbf{y} \setminus \mathbf{x})\, p(\mathbf{x})}{\int_X p(\mathbf{y} \setminus \mathbf{x})\, p(\mathbf{x}) d\mathbf{x}} \tag{3.18}$$

There are two generally used estimators. These are minimum mean square error (MMSE) estimator and maximum a posteriori (MAP) estimator. In MMSE, the mean square of the error is minimized. In mathematical terms:

$$E\left[(\mathbf{x}-\hat{\mathbf{x}})^2\right] = \int (\mathbf{x}-\hat{\mathbf{x}})^2 \, p(\mathbf{y},\mathbf{x}) d\mathbf{y} d\mathbf{x} \tag{3.19}$$

where $\hat{\mathbf{x}}$ is the estimate of unknown, **x**. Theoretically, we take average of the squared error with respect to joint pdf p(**y,x**). Then, we can write the estimator for MMSE as:

$$\hat{\mathbf{x}} = \int_{\mathbf{x}} \mathbf{x} \, p(\mathbf{x} \setminus \mathbf{y}) d\mathbf{x} \tag{3.20}$$

For MAP estimation, we maximize the posterior pdf p(**x****y**):

$$\hat{\mathbf{x}} = \arg \max_{\mathbf{x}} p(\mathbf{x} \setminus \mathbf{y}) \tag{3.21}$$

We observe that the denominator in (3.18) is the normalization part. Therefore, (3.21) is equivalent to:

$$\hat{\mathbf{x}} = \arg \max_{\mathbf{x}} p(\mathbf{y} \setminus \mathbf{x}) p(\mathbf{x}) \tag{3.22}$$

A special case, n is a white Gaussian noise (WGN) with zero mean $\mathbf{n} \sim N(0, \mathbf{C_n})$ and independent of **x**, A is the known matrix, and x is the random vector with prior pdf $N(\overline{\mathrm{x}}, \mathbf{C_X})$. When the random variables **y** and **x** are jointly Gaussian then the posterior pdf is also Gaussian. For representation of posterior pdf p(**x****y**), only the mean and covariance is sufficient.

$$E[\mathbf{y}] = E[\mathbf{A}\mathbf{x} + \mathbf{n}] = \mathbf{A}E[\mathbf{x}] = \mathbf{A}\bar{\mathbf{x}} \tag{3.23}$$

$$E[\mathbf{x}] = \bar{\mathbf{x}} \tag{3.24}$$

$$\begin{aligned} \mathbf{C}_{\mathbf{yy}} &= E[(\mathbf{y} - \bar{\mathbf{y}})(\mathbf{y} - \bar{\mathbf{y}})^T] \\ &= \mathbf{A}\mathbf{C}_{\mathbf{x}}\mathbf{A}^T + \mathbf{C}_{\mathbf{n}} \end{aligned} \tag{3.25}$$

The cross-covariance is

$$\mathbf{C}_{\mathbf{xy}} = E[(\mathbf{x} - \bar{\mathbf{x}})(\mathbf{y} - \bar{\mathbf{y}})^T] = \mathbf{C}_{\mathbf{x}}\mathbf{A}^T \tag{3.26}$$

Then from theorem 10.3 in [52] the posterior pdf is Gaussian with mean

$$E[\mathbf{x} \mid \mathbf{y}] = \bar{\mathbf{x}} + \mathbf{C}_{\mathbf{x}}\mathbf{A}^T(\mathbf{A}\mathbf{C}_{\mathbf{x}}\mathbf{A}^T + \mathbf{C}_{\mathbf{n}})^{-1}(\mathbf{y} - \mathbf{A}\bar{\mathbf{x}}) \tag{3.27}$$

And covariance

$$\mathbf{C}_{\mathbf{x}|\mathbf{y}} = \mathbf{C}_x - \mathbf{C}_{\mathbf{x}}\mathbf{A}^T(\mathbf{A}\mathbf{C}_{\mathbf{x}}\mathbf{A}^T + \mathbf{C}_{\mathbf{n}})^{-1}\mathbf{A}\mathbf{C}_{\mathbf{x}} \tag{3.28}$$

or

$$\mathbf{C}_{\mathbf{x}|\mathbf{y}} = (\mathbf{C}_{\mathbf{x}}^{-1} + \mathbf{A}\mathbf{C}_{\mathbf{n}}\mathbf{A}^T)^{-1} \tag{3.29}$$

In the MAP solution the posterior pdf should be maximized. For the Gaussian assumption case, the MMSE and MAP solutions coincide. More details are given in [52].

Assuming that $\mathbf{x}$ has normal distribution with mean $\bar{\mathbf{x}}$ and covariance $\mathbf{C_x}$ and noise characteristics are $\mathrm{n} \sim \mathrm{N}(0, \mathrm{C_n})$, the MAP or MMSE solution is:

$$\hat{\mathbf{x}} = (\mathbf{A}^T \mathbf{C_n}^{-1} \mathbf{A} + \mathbf{C_x}^{-1})^{-1} (\mathbf{A}^T \mathbf{C_n}^{-1} \mathbf{y} + \mathbf{C_x}^{-1} \bar{\mathbf{x}}) \tag{3.30}$$

In this study, we assume the unknown is zero mean ($\bar{\mathbf{x}} = 0$). Then, we can rearrange (3.30) as:

$$\hat{\mathbf{x}} = (\mathbf{A}^T \mathbf{C_n}^{-1} \mathbf{A} + \mathbf{C_x}^{-1})^{-1} \mathbf{A}^T \mathbf{C_n}^{-1} \mathbf{y} \tag{3.31}$$

We can also rewrite (3.21) using the matrix inversion lemma [52] and restate the MAP estimate as:

$$\hat{\mathbf{x}} = \mathbf{C_x} \mathbf{A}^T (\mathbf{A} \mathbf{C_x} \mathbf{A}^T + \mathbf{C_n})^{-1} \mathbf{y} \tag{3.32}$$

The critical point in the Bayesian method is choice of a prior pdf. If we choose the wrong prior, the estimator is bad and not optimal. We choose prior that has a Gaussian pdf.

### 3.2.4 Solution Approaches

In the previous section, we have explained the essential tools for solving the inverse ECG problem. In this section, we explain the approaches that are employed to use these methods. There are two main approaches. We can classify these approaches whether the temporal correlation is imposed into the solution or not. The traditional way is the column sequential approach. As a second alternative, we examine direct solution when temporal information is used. As a final approach, we use temporal whitening.

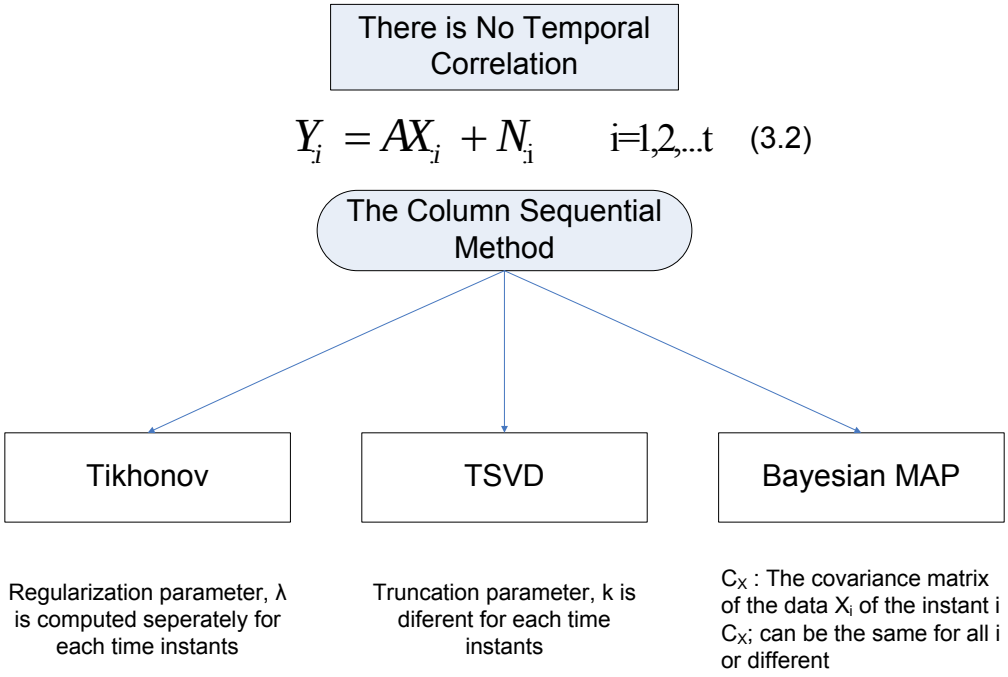


Figure 3.2 : The schematic of the process when there is no temporal correlation

Firstly, we explained how we can solve the problem without imposing the temporal correlation. The mostly used method is the column sequential method that requires some assumptions [2] (Figure 3.2). These assumptions allow us solve the problem separately for each time instants.

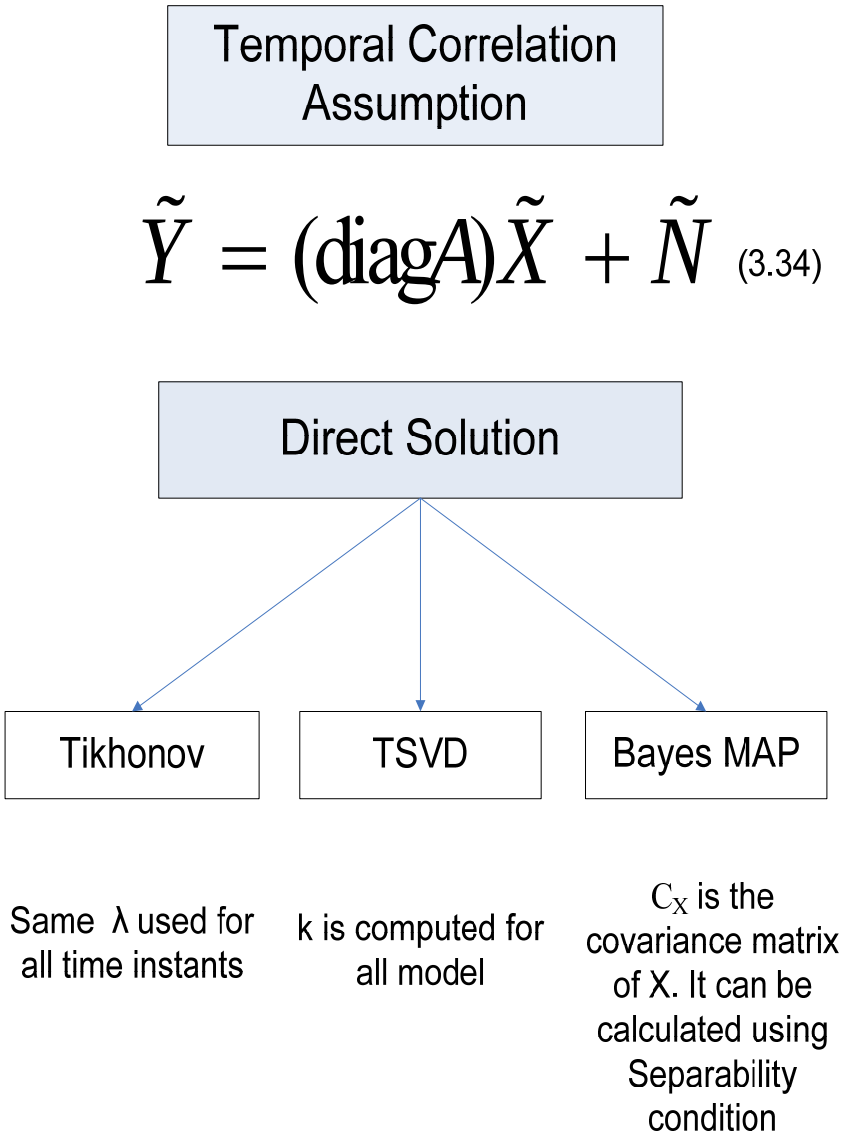


Figure 3.3 : The schematic representation of the direct solution

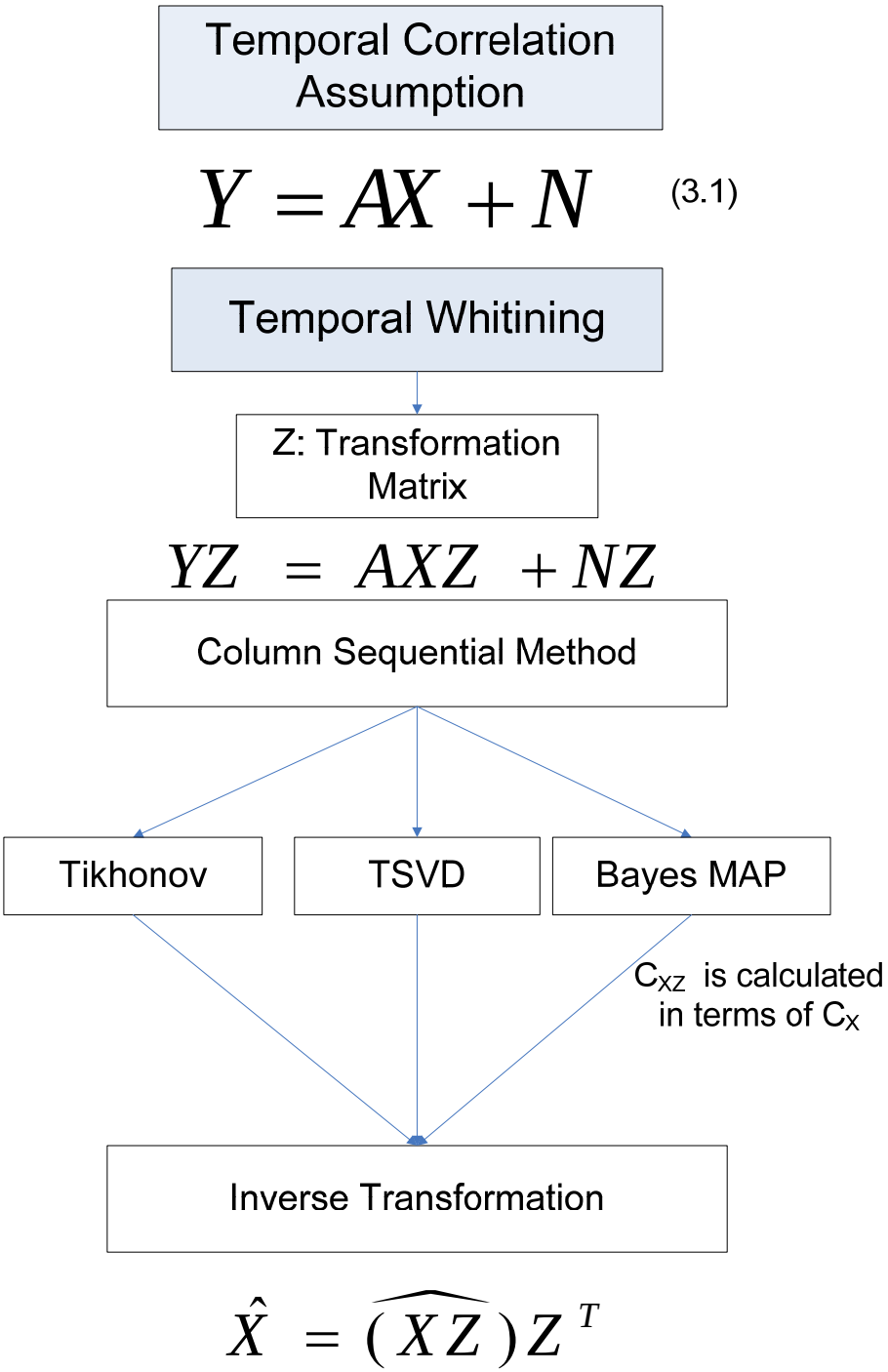


Figure 3.4 : The Schematic representation of Temporal Whitening

Secondly, we clarified the situation that the temporal correlation added to the solution. There are two techniques: Direct solution and temporal whitening. In the direct solution, we apply the essential methods to entire system. All computations and calculations of parameters are taken place with respect to entire system (regularization parameter etc.). In the spatio-temporal Bayesian MAP approaches, we use the separability condition to define the covariance matrix of **X**, which involves the separation of the temporal and spatial components of the covariance matrix (Figure 3.3). In the temporal whiting, the domain of the solution is changed in order to decorrolating the problem for applying column sequential method (Figure 3.4).

#### 3.2.4.1 Solution Approach Without Temporal Correlation

The main idea of this approach is independence of the measurement for different time instants. Therefore, we can separate the matrix equation (3.1) into linear equations for each time instant as in equation (3.3). Then we can solve the system for each time instants independently. Thus, it is called the column sequential approach (ColSeq).

Implementing this approach by using TSVD and Tikhonov regularization does not contain spatial or temporal correlation. However, in Bayesian estimation, it involves spatial correlation due to the nature of Bayesian theory.

Then we can solve the problem for each time instant by using appropriate methods that are explained before (Figure 3.2).

In Tikhonov regularization, the regularization parameter is calculated separately for each time instant. In the same way, TSVD is applied to equations (3.3) separately with different truncation parameters for each time instant. In Bayesian MAP, we apply (3.32) to the (3.3) at each time instant. Here the covariance matrix, $\mathbf{C_X}$ is the spatial covariance matrix of epicardial vector **x** at each time instant. We have two choices for $\mathbf{C_X}$**.** It can be the same for all time instants or it can be calculated separately for each time instant.

This approach is the easiest and fastest solution procedure. However, this has not realistic results since uncorrelatedness assumption has been broken due to the nature of problem. We know that there is a relation between the potential of different nodes at different time instants.

#### 3.2.4.2 Temporal Correlation Assumption

For imposing temporal dynamics of the problem into the solution, we can use direct approach and temporal whitening approach.

***Direct Solution***

Let us write equation (3.2) again:

$$\underbrace{\begin{bmatrix}\mathbf{Y}_{:1}\\ \vdots \\ \mathbf{Y}_{:t}\end{bmatrix}}_{\tilde{\tilde{\mathbf{Y}}}} = \underbrace{\begin{bmatrix}\mathbf{A} & & \mathbf{0}\\ & \ddots & \\ \mathbf{0} & & \mathbf{A}\end{bmatrix}}_{\text{diag}\mathbf{A}} \cdot \underbrace{\begin{bmatrix}\mathbf{X}_{:1}\\ \vdots \\ \mathbf{X}_{:t}\end{bmatrix}}_{\tilde{\tilde{\mathbf{X}}}} + \underbrace{\begin{bmatrix}\mathbf{N}_{:1}\\ \vdots \\ \mathbf{N}_{:t}\end{bmatrix}}_{\tilde{\tilde{\mathbf{N}}}} \tag{3.33}$$

or in a simplified way:

$$\tilde{\mathbf{Y}} = (\text{diag}\mathbf{A})\tilde{\mathbf{X}} + \tilde{\mathbf{N}} \tag{3.34}$$

In the direct solution, we try to solve (3.34) directly for the entire system. Applying Tikhonov regularization and TSVD on equation (3.34) is theoretically difficult. The regularization parameter, λ for Tikhonov regularization and truncation parameter, k for TSVD are computed for entire system represented by (3.33). For Bayesian approach, we apply equation (3.32) to the system that is represented by (3.34). We assume that we have Gaussian zero mean prior pdf. Then the solution is:

$$\hat{\tilde{\mathbf{X}}} = \mathbf{C}_{\tilde{\mathbf{X}}}(\text{diag}\mathbf{A})^T[(\text{diag}\mathbf{A})\mathbf{C}_{\tilde{\mathbf{X}}}(\text{diag}\mathbf{A}^T) + \mathbf{C}_{\tilde{\mathbf{N}}}]^{-1}\tilde{\mathbf{Y}} \tag{3.35}$$

The covariance matrices can represented by:

$$\mathbf{C}_{\tilde{\mathbf{X}}} = (E[\mathbf{X}_{:i}\mathbf{X}_{:j}^T])_{i,j} \tag{3.36}$$

$$\mathbf{C}_{\tilde{\mathbf{N}}} = (E[\mathbf{N}_{:i}\mathbf{N}_{:j}^T])_{i,j} \tag{3.37}$$

In this notation $[]_{i,j}$ is represents ij$^{th}$ block of the matrix, and $E[.]$ is the expected value.

For the direct solution, we create the covariance matrix $C_X$ that is a full matrix. However, because of the high-dimensionality of the problem posed in (3.33), it is

too difficult to implement. Alternatively, we can use the separability condition for forming the the covariance matrix $C_X$. In this form, we suggest several statistical assumptions [44].

In Bayesian estimation, we can represent the covariance matrix separately in terms of its spatial covariance and temporal covariance. This is called the separability condition [44]. Using this condition, the covariance matrix can be separated into two parts:

$$\mathbf{C_X} = \mathbf{C_t} \otimes \mathbf{C_s} \tag{3.38}$$

where $C_t$ and $C_s$ are the temporal covariance matrix and spatial covariance matrix respectively; $\otimes$ represents the Kronecker product. The main idea comes from Greensite's isotropy assumption [44]. The isotropy assumption is the dual of separability in the random matrix theory. The covariance matrix $C_X$ can be partially or completely described from the measurements itself [44]. The spatial and temporal covariance matrices in (3.38) are represented as: $C_{s_{i,j}} = C_s(i,j)$, ij$^{th}$ element of $C_s$ and $C_{t_{u,v}} = C_t(u,v)$, uv$^{th}$ element of $C_t$ . The total temporal covariance matrix is $E[X^TX]$ and the total spatial covariance matrix is $E[XX^T]$ then their mathematical formulation for mean-removed unknown, X is:

$$E[\mathbf{X}^T\mathbf{X}] = C_t.\sum_{v=1}^{p} C_s(s_v, s_v) \quad \text{and} \quad E[\mathbf{X}\mathbf{X}^T] = C_s.\sum_{i=1}^{t} C_t(t_i, t_i) \tag{3.39}$$

Then if (3.38) and (3.39) are combined, the covariance matrix can be represented in a Kronocker product form as follows [44]:

$$\mathbf{C}_{\mathbf{X}} = \frac{E[\mathbf{X}^T\mathbf{X}] \otimes E[\mathbf{X}\mathbf{X}^T]}{\sum_v^m C_s(v,v).\sum_{i=1}^t C_t(i,i)} \tag{3.40}$$

Using the relationship

$$\sum_{v=1}^{m} C_s(v,v).\sum_{i=1}^{t} C_t(i,i) = tr(E[\mathbf{X}^T\mathbf{X}]) = tr(E[\mathbf{X}\mathbf{X}^T]) = E[\|\mathbf{X}\|_F^2] \tag{3.41}$$

where $\|.\|_F$ is the Frobenius norm (more details in AppendixA), equation (3.40) can be simplified as:

$$\mathbf{C}_{\mathbf{X}} = \frac{E[\mathbf{X}^T\mathbf{X}] \otimes E[\mathbf{X}\mathbf{X}^T]}{E([\|\mathbf{X}\|_F^2])} \tag{3.42}$$

This is the main formulation for "separability condition". This equation can be used for the direct method substituting in (3.32) for vector notation of X. However, dimension of the $C_X$ becomes too large due to the vector notation. Thus, we use the other alternative to add temporal information, temporal whitening.

### *Temporal Whitening*

In this section, we explain the temporal whiting. This method is proposed for improving the results of column sequential methods by decreasing error that occurs by ignoring temporal dynamics of the problem. In this method, the system

is decorrelated with the assumptions, and then we apply the column sequential method. It is equivalent to applying smoothing filter to the problem.

In column sequential method (in section 3.2.1), we have supposed that there is no correlation between different time instants [2]. However, this assumption has been proved wrong due to the nature of the problem. If the $C_X$ is chosen a full matrix, it involves both spatial and temporal information about the model.

For simplicity, the noise N can be regarded as independent and identically distributed (i.i.d.).

$$E[\mathbf{N}_{:i}\mathbf{N}_{:j}^{T}] = \sigma_N^2 \delta_{ij} \tag{3.43}$$

Therefore the noise covariance matrix is a diagonal matrix.

Under these assumptions, in this approach, one needs to find a transformation matrix to change the solution coordinates for supplying the independency. Firstly, we created the transformation matrix Z. Its properties will be explained later. Then, we apply to (3.1) and (3.32):

$$\mathbf{YZ} = \mathbf{AXZ} + \mathbf{NZ} \tag{3.42}$$

$$\begin{pmatrix} \widehat{\mathbf{XZ}}_{:1} \\ \vdots \\ \widehat{\mathbf{XZ}}_{:t} \end{pmatrix} = \mathbf{C_{XZ}}(\mathrm{diag}\mathbf{A})^{T}[(\mathrm{diag}\mathbf{A})\mathbf{C_{XZ}}(\mathrm{diag}\mathbf{A})^{T} + \mathbf{C_{NZ}}]^{-1} \begin{pmatrix} \mathbf{YZ}_{:1} \\ \vdots \\ \mathbf{YZ}_{:t} \end{pmatrix} \tag{3.44}$$

where $\mathbf{C_{XZ}} = (E[(\mathbf{XZ})_{:i}(\mathbf{XZ})_{:j}^T])_{i,j}$ and $\mathbf{C_{NZ}} = (E[(\mathbf{NZ})_{:i}(\mathbf{NZ})_{:j}^T])_{i,j}$. The solution $\widehat{\mathbf{XZ}}$ is optimal if $\mathbf{C_{XZ}}$ and $\mathbf{C_{NX}}$ are block diagonal. Using the homogeneity assumption provided in [2] and replacing **X, Y, N** with **XZ, YZ, NZ**, we rewrite the equations for the covariance matrix.

The off-diagonal block matrices are:

$$E[\mathbf{XZ}_{:i}(\mathbf{XZ})_{:j}^T] = \frac{E[\mathbf{YZ}_{:i}.\mathbf{YZ}_{:j}]}{tr(\mathbf{A}^T\mathbf{A})} = \frac{(\mathbf{Z}_{:i})^T E[\mathbf{Y}_{:i}.\mathbf{Y}_{:j}]\mathbf{Z}_{:j}}{tr(\mathbf{A}^T\mathbf{A})} \qquad \text{for } i \neq j \qquad (3.45)$$

If we choose Z that is an orthogonal matrix that diagonalizes $E[Y^TY]$, the covariance matrices $C_{XZ}$ and $C_{NZ}$ are block diagonal, since entries of $E[Y^TY]$ are zero for $i \neq j$. Furthermore, the matrices at the diagonal can be represented as:

$$E[(\mathbf{XZ})_{:i}(\mathbf{XZ})_{:j}^T] = \frac{(\mathbf{Z}_{:i})^T (E[\mathbf{Y}_{:i}.\mathbf{Y}_{:j}] - E[\mathbf{N}_{:i}.\mathbf{N}_{:j}])\mathbf{Z}_{:j}}{tr(\mathbf{A}^T\mathbf{A})} \qquad \text{for } i = j \qquad (3.46)$$

Under these assumptions, we can apply column sequential method to the problem:

$$\mathbf{YZ}_{:i} = \mathbf{A}(\mathbf{XZ})_{:i} + \mathbf{NZ}_{:i} \qquad (3.47)$$

After solving these equations instead of the huge system of linear equations, we should move back to the real domain. Since the orthogonal matrix supplies $ZZ^T=I$, the optimal solution can be found as:

$$\hat{\mathbf{X}} = \widehat{(\mathbf{XZ})}\mathbf{Z}^T \tag{3.48}$$

The question is how this transformation matrix can be chosen. It is only required that the transformation matrix Z is orthogonal and it diagonalizes E[$\mathbf{Y}^T\mathbf{Y}$]. The basic choice of Z that supplies these specifications is the eigenvectors of the E[$\mathbf{Y}^T\mathbf{Y}$]. Since we know that eigenvectors are orthogonal vectors and they diagonalize the matrix from linear algebra literature. All the proofs and the other lemmas that are used are referenced [44].

Briefly, we apply temporal whiting in order to impose the temporal dynamics to the problem by applying the column sequential method after decorrelation of the problem. Firstly, we scaled the problem with the eigenvectors of E[$\mathbf{Y}^T\mathbf{Y}$]. Then the new equation system is solved in its domain. Lastly, we go back to original domain.

#### 3.2.4.3 Separable Bayes Column Sequential:

The last approach is the combination of the temporal whitening and separable condition. In usual way, these methods can be used together. However, high dimensionality cause result in long run time in the simulation. We proposed a new method that accelerate the algorithm and prevent loss of time. Firstly, we rewrite the $\mathbf{C_{XZ}}$ after scaling the problem by Z in terms of $\mathbf{C_X}$. Then we use it in the equation (3.44).

In usual way, we can write the $\mathbf{C_{XZ}}$ by replacing **X** with **XZ** in the equation (3.40):

$$\mathbf{C}_{\mathbf{XZ}} = \frac{E[(\mathbf{XZ})^T \mathbf{XZ}] \otimes E[\mathbf{XZ}(\mathbf{XZ})^T]}{E([\|\mathbf{XZ}\|_F^2])} \tag{3.49}$$

Firstly, we search the expectations on numerator of the equation above.

$$E[(\mathbf{XZ})^T \mathbf{XZ}] = E[\mathbf{Z}^T(\mathbf{X}^T\mathbf{X})\mathbf{Z}] = \mathbf{Z}^T E[\mathbf{X}^T\mathbf{X}]\mathbf{Z} \tag{3.50}$$

$$E[\mathbf{XZ}(\mathbf{XZ})^T] = E[\mathbf{X}(\mathbf{ZZ}^T)\mathbf{X}^T] \tag{3.51}$$

From previous section, for any matrix $M \in R^{m\times m}$, we can write (3.45). Therefore, we can arrange (3.51).

$$E[\mathbf{XZ}(\mathbf{XZ})^T] = \frac{tr(\mathbf{ZZ}^T)}{t} E[\mathbf{XX}^T] \tag{3.52}$$

where t indicates the number of time instants or the length of **X** and **Y** in (1).

For the numerator in (3.49), from the definition of the Frobenius norm:

$$E([\|\mathbf{XZ}\|_F^2]) = tr((\mathbf{XZ})^T \mathbf{XZ}) = tr(\mathbf{Z}^T(\mathbf{X}^T\mathbf{X})\mathbf{Z}) \tag{3.53}$$

Using the property of trace operation (B6):

$$tr(Z^T(X^T X)Z) = tr(X^T X) \tag{3.54}$$

3.54 follows 3.53, since we choose Z as a eigenvector of $E[Y^TY]$ that is an orthogonal transformation known from linear algebra, the Frobenius matrix norm is invariant under orthogonal transformation. (The detailed information about Frobenius norm and trace is given in Appendix B.) Therefore,

$$E([\|\mathbf{XZ}\|_F^2]) = E([\|\mathbf{X}\|_F^2]) \tag{3.55}$$

Now, (3.50), (3.52) and (3.55) are replaced in (3.49)

$$\mathbf{C_{XZ}} = \frac{(\mathbf{Z}^T E[\mathbf{X}^T\mathbf{X}]Z) \otimes \frac{tr(\mathbf{ZZ}^T)}{t} E[\mathbf{XX}^T]}{E([\|\mathbf{X}\|_F^2])} \tag{3.56}$$

Applying property of the Kronecker product in (A2), (3.56) becomes

$$\mathbf{C_{XZ}} = \frac{tr(\mathbf{ZZ}^T)}{t} . \frac{(\mathbf{Z}^T E[\mathbf{X}^T\mathbf{X}]Z) \otimes (E[\mathbf{XX}^T])}{E([\|\mathbf{X}\|_F^2])} \tag{3.57}$$

(3.57) can be written as:

$$\mathbf{C_{XZ}} = \frac{tr(\mathbf{ZZ}^T)}{t} . \frac{(\mathbf{Z}^T E[\mathbf{X}^T\mathbf{X}]\mathbf{Z}) \otimes (\mathbf{I}_n . E[\mathbf{XX}^T] . \mathbf{I}_n)}{E([\|\mathbf{X}\|_F^2])} \tag{3.58}$$

where $\mathbf{I_n}$ is the $n \times n$ identity matrix

Under the property of Kronecker product (A7), (3.68) can be rewritten

$$\mathbf{C}_{\mathbf{XZ}} = \frac{tr(\mathbf{Z}\mathbf{Z}^T)}{t}.\frac{(\mathbf{Z}^T \otimes \mathbf{I}_n)(E[\mathbf{X}^T\mathbf{X}] \otimes E[\mathbf{X}\mathbf{X}^T])(\mathbf{Z} \otimes \mathbf{I}_n)}{E([\|\mathbf{X}\|_F^2])} \tag{3.59}$$

or

$$\mathbf{C}_{\mathbf{XZ}} = \frac{tr(\mathbf{Z}\mathbf{Z}^T)}{t}.(\mathbf{Z}^T \otimes \mathbf{I}_n).\frac{(E[\mathbf{X}^T\mathbf{X}] \otimes E[\mathbf{X}\mathbf{X}^T])}{E([\|\mathbf{X}\|_F^2])}.(\mathbf{Z} \otimes \mathbf{I}_n) \tag{3.60}$$

At the beginning of part 3.2.4.2, the separable condition has been explained; we define the $\mathbf{C_X}$ as in (3.38). Then we can replace the middle part in the right side of (3.60) with $\mathbf{C_X}$. The final equation has been obtained.

$$\mathbf{C}_{\mathbf{XZ}} = \frac{tr(\mathbf{Z}\mathbf{Z}^T)}{t}.(\mathbf{Z}^T \otimes \mathbf{I}_n).\mathbf{C}_{\mathbf{X}}.(\mathbf{Z} \otimes \mathbf{I}_n) \tag{3.61}$$

At the end, we can rewrite $C_{XZ}$ in terms of $C_X$. Consequently, if $C_X$ is known, one does not need to calculate $\mathbf{C_{XZ}}$ classically. This gives a chance to accelerate the procedure and decrease memory requirements. After this statement, we can solve the problem using (3.44) and (3.47) together.

In summary, in this chapter we explained how the ECG inverse problem can be solved although the questions come from the nature of the problem and

complexity. We investigated deeply the methods and approaches that are used. In addition, we stated the contribution of the study. We combined two approaches to speed up and ease the procedure. In the next part, we will give our simulation results to compare the methods and approaches.

# CHAPTER 4

## RESULTS AND DISCUSSION

In this section, we tested and compared the methods introduced in the previous section. The results were interpreted at end of the section. In the simulation, we used three different data sets. Two of them were synthetic data that are generated by using specifications from publications [2] [44]. The last one involved epicardial measurements obtained by Dr. Robert S. MacLeod at University of Utah, Nora Eccles Cardiovascular Research and Training Institute (CVRTI). In the first two examples, we gave the mesh graphs of the original data and its estimates obtained with various methods for illustration. In the realistic torso simulation with real epicardial potential measurements, we used 3D geometrical visualization software, map3d [56] to display the epicardial potential maps. For quantitative comparison of methods, we used two criteria; relative error (RE) and the correlation coefficient.

In all our simulations, we knew the true (desired) solution matrix, **X**. To obtain the perturbed data matrix, **Y**, we first multiplied the true solution matrix, **X**, and the transfer matrix, **A**, and then added white Gaussian noise (WGN) noise at 30 dB SNR. We used the matrix **Y** as input and estimated the unknown signal matrix **X** by using a suitable inverse problem technique (Figure 4.1).

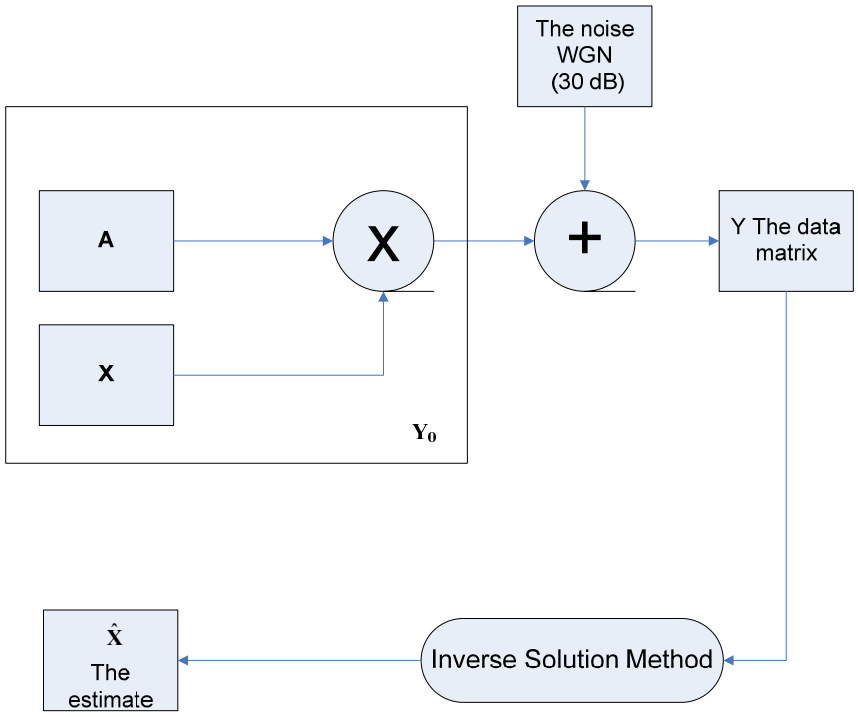


Figure 4.1 : The schematic representation of the simulation procedure

### 4.1 Data Sets

In this section, we present the data used for testing the performances of the applied methods.

#### 4.1.1 Synthetic Data

a) Data 1

The experimental procedure is analogous with EEG problem [2]. The data matrix **Y** corresponds to time-varying scalp potentials at different measurement locations. The transfer matrix, **A**, is a general ill-conditioned smoothing matrix.

The space-time signal matrix, **X**, contains two spikes (figure 4.2). The entries of the signal matrix **X** are calculated as:

$$\mathbf{X}_{ij} = \frac{6}{2+(i-10)^2+(j-9)^2} + \frac{6}{2+(i-3)^2+(j-6)^2} \qquad \text{i,j} = 1,2,.....,15 \qquad (4.1)$$

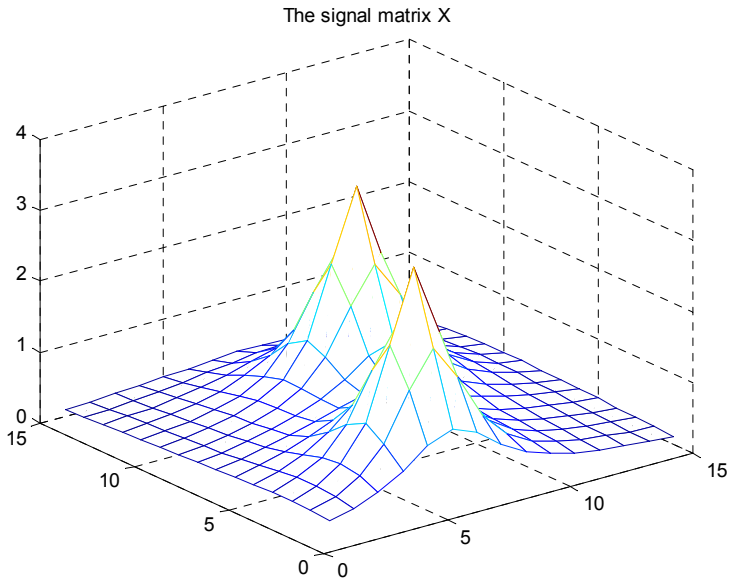


Figure 4.2 : The signal matrix, X

The transfer matrix, **A** is a Toeplitz matrix whose entries are given by:

$$\mathbf{A}_{ij} = \gamma^{(|i-j|)^{\mu}} \qquad \text{i,j} = 1,2,.....15\,. \qquad (4.2)$$

Here, the parameters are set to $\gamma$=1.5 and $\mu$=0.9. The model is formed by using the formula in (3.1). The noise is WGN at 30dB SNR.

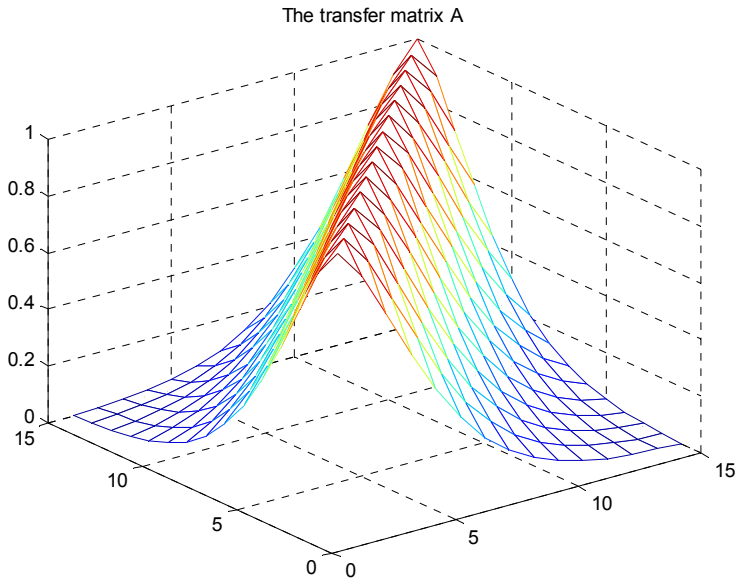


Figure 4.3 : The transfer matrix, A

b) Data 2

In this model, we have a curve with two Gaussian-shaped peaks, which moves from left to right [44]. At the initial time instant, the curve is defined as:

$$x(n) = \frac{1}{2}\frac{1}{\sqrt{2\pi}}\exp\left(-\frac{(n-m_1)^2}{2\sigma^2}\right) + \frac{1}{4}\frac{1}{\sqrt{2\pi}}\exp\left(-\frac{(n-m_2)^2}{2\sigma^2}\right) \qquad \text{n=1,2,...,128} \quad (4.3)$$

The initial mean and standard deviation of the peaks is set to $[m_1, \sigma_1] = [20, 7]$ and $[m_2, \sigma_2] = [70, 17]$.

The behavior of the curve follows the state-space model form:

$$\mathbf{x}_i = (\mathbf{H} + \varepsilon \mathbf{I}_N)\mathbf{x}_{i-1} + \mathbf{u}_i \tag{4.4}$$

where H, the fixed state-transition matrix, is one-step circular shift permutation matrix in the form:

$$H = \begin{bmatrix} 0 & \cdots & & 0 & 1 \\ 1 & & & & 0 \\ 0 & \ddots & & & \vdots \\ \vdots & & \ddots & & \\ 0 & \cdots & 0 & 1 & 0 \end{bmatrix} \tag{4.5}$$

This matrix **H** is distorted by a random noise $\varepsilon \sim N(0.01^2)$, which is the model error. The prediction noise is small, $\mathbf{u} \sim N(0, 0.01^2)$. The curve, *x(n)*, is calculated for 40 time instants using (4.4). The initial and final curves are shown in Figure 4.4.

The forward transfer matrix, A is a 128×128 convolution matrix with a Gaussian Kernel, whose components are given as:

$$A(i, j) = \frac{1}{N}\frac{1}{\sqrt{2\pi}\sigma}\exp\left(\frac{\left(\frac{i-j}{N}\right)^2}{2\sigma^2}\right) \quad \text{i,j} = 1,2,\ldots,128 \tag{4.6}$$

where N=128 and σ=0.136. The matrix A is ill-conditioned with small condition number. For generating the model, we use again the same linear model in (3.1). The noise is WGN at 30dB SNR.

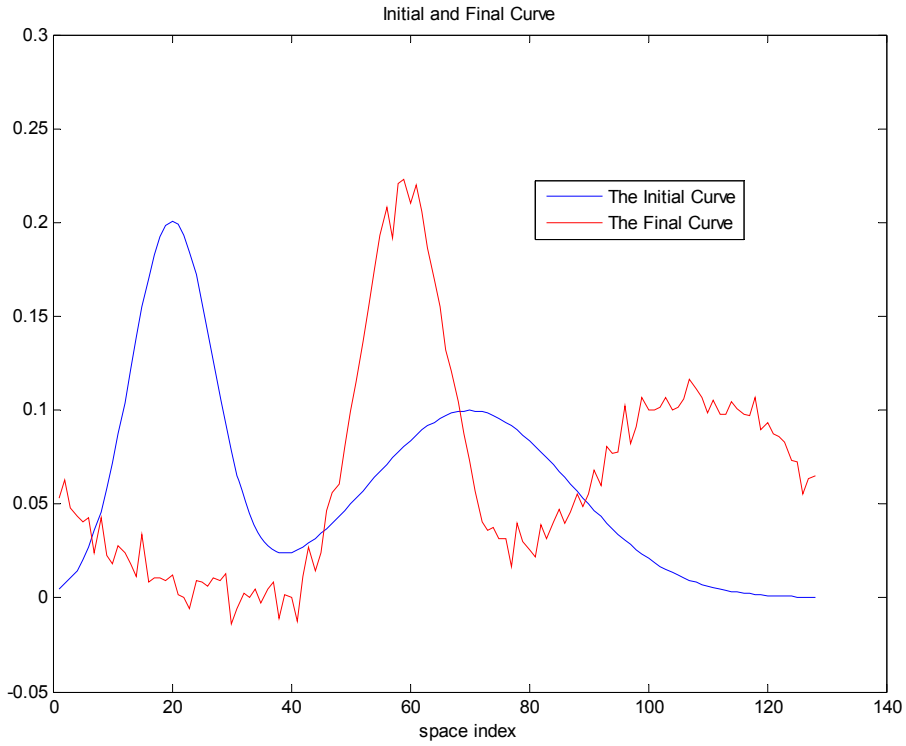


Figure 4.4 : The illustration of the initial and final curves Data 2 with two Gaussian-shaped peaks

### 4.1.2 Simulated Torso Measurements

In this experiment, we used the data obtained by Robert S. MacLeod in University of Utah, Nora Eccles CVRTI. They used a human torso tank made of fiberglass with a realistic shape of an adolescent [57]. It is filled with electrolyte of a realistic conductivity (500 Ωcm). An isolated canine heart is suspended in the tank.

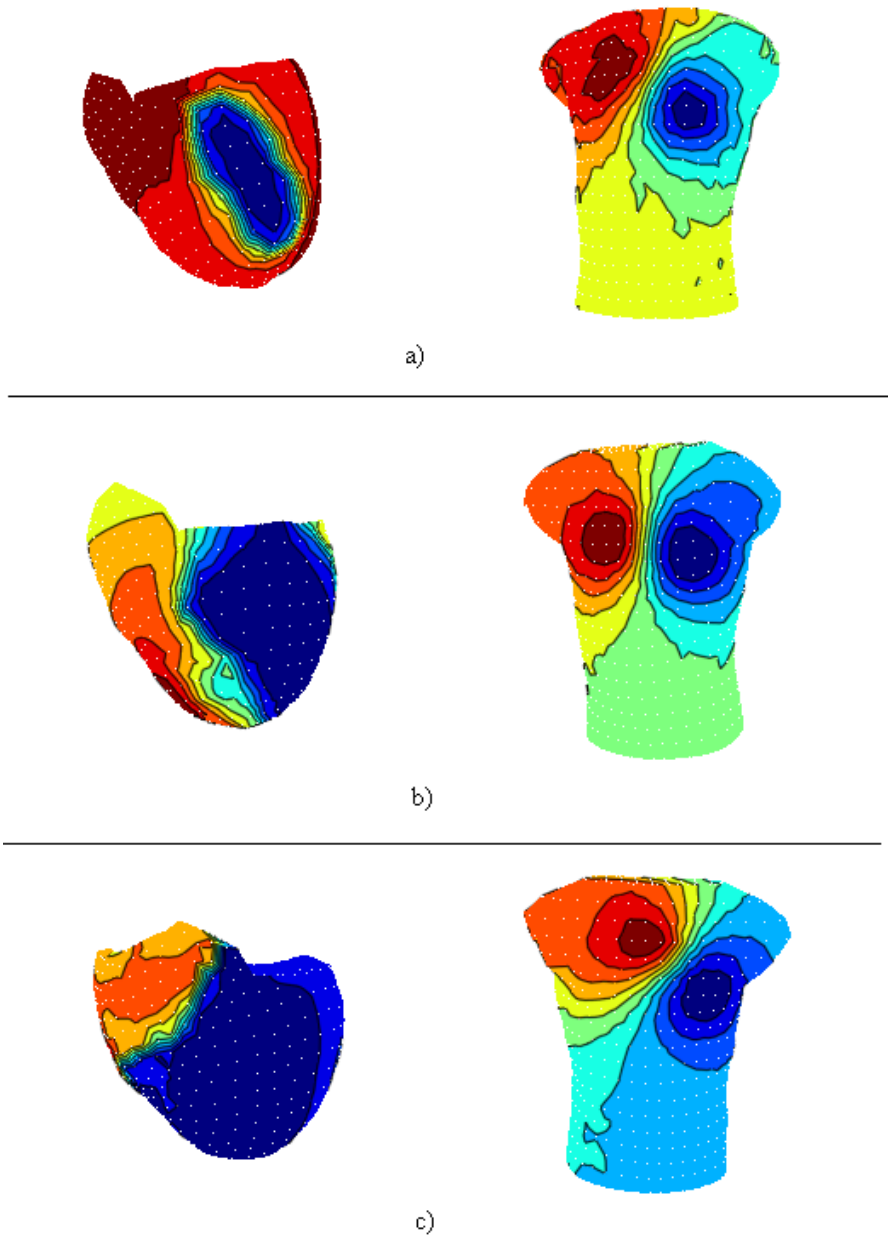


Figure 4.5 : The epicardial and torso potentials are recorded at a) 29 ms. b) 59 ms. c) 86 ms.

A sock electrode array that contains 490 electrodes is used for the acquisition of epicardial potentials. The forward transfer matrix is solved for the homogeneous

torso using boundary element method (BEM). We obtained the torso potentials used in this simulation by adding WGN at 30 dB SNR to the multiplication of epicardial potentials and forward transfer matrix. There are 771 nodes on the torso surface. Only the QRS complex of the measured signal is taken into account (109 ms.-109 time instants). Figure 4.5 shows the torso and the epicardial potential distributions at three different time instants.

## 4.2 Methods

In the simulations, we use seven methods:

*No temporal Correlation*:

- Tikhonov regularization (Tikh)
- TSVD
- Bayesian MAP estimation (Bayes)

*Temporal Correlation Assumption*:

- Tikhonov with temporal whitening (TikhTemp)
- TSVD with temporal whitening (TSVDTemp)
- Bayesian MAP with temporal whitening (BayesTemp)
- Bayesian MAP direct solution (BayesDirect)
- Tikhonov direct solution (TikhDirect)
- TSVD direct solution (TSVDDirect)

The first six methods were applied to simulations of all three data sets. The remaining three could not be applied on the simulated torso potentials because of high dimensions of the problem, they only used for the other data sets.

The regularization parameter, λ in Tikhonov regularization and the truncation parameter, k in TSVD are chosen with minimum RE condition from a given interval.

### 4.3 Evaulation Criteria

For evaulation, we use two criteria. The first one is the relative error, that is defined in the previous chapter with equation (3.10). It gives the error with respect to original data. The second one is correlation coefficient that represents how the estimation resembles to the original one. It is define as:

$$r_{XY} = \frac{C_{XY}}{\sigma_X \sigma_Y} \tag{4.7}$$

where $C_{XY}$ is the cross-covariance matrix and $\sigma_X$, $\sigma_Y$ are the standard deviation of X and Y respectively.

For 3D visualization, we use a geometry displaying software, map3d that is obtained from Scientific Computing and Imaging (SCI) Institute at University of Utah. By means of this software, we can display the measured data on a 3D geometry.

## 4.4 Results

### 4.4.1 Experiment 1 with Data 1

In this example, we use the first data set described in section 4.1.1 – a) [2]. The error performances and correlation coefficients are compared in the Figure 4.6 and Figure 4.7, respectively. The noise performance is given in table 4.1. The 3D visualizations of the solutions corresponding to each method are shown in Figure 4.8.

Table 4.1 : The average value and standard deviation of the relative error

| SNR (dB) | 30 | 18 | 9.6 | 4.8 | 2.4 |
|---|---|---|---|---|---|
| Tikh | 0.257 ± 0.075 | 0.245 ± 0.081 | 0.357 ± 0.104 | 0.371 ± 0.134 | 0.499 ± 0.156 |
| TikhTemp | 0.237 ± 0.082 | 0.254 ± 0.110 | 0.321 ± 0.097 | 0.443 ± 0.180 | 0.525 ± 0.142 |
| TikhDirect | 0.225 ± 0.112 | 0.314 ± 0.106 | 0.446 ± 0.189 | 0.495 ± 0.100 | 0.617 ± 0.202 |
| TSVD | 0.209 ± 0.046 | 0.206 ± 0.069 | 0.355 ± 0.095 | 0.489 ± 0.210 | 0.492 ± 0.187 |
| TSVDTemp | 0.222 ± 0.069 | 0.269 ± 0.127 | 0.355 ± 0.124 | 0.526 ± 0.329 | 0.581 ± 0.331 |
| TSVDDirect | 0.190 ± 0.080 | 0.250 ± 0.070 | 0.368 ± 0.100 | 0.599 ± 0.347 | 0.650 ± 0.380 |
| Bayes | 0.297 ± 0.099 | 0.344 ± 0.119 | 0.423 ± 0.167 | 0.751 ± 0.272 | 0.811 ± 0.560 |
| BayesTemp | 0.283 ± 0.110 | 0.309 ± 0.073 | 0.402 ± 0.092 | 0.481 ± 0.088 | 0.510 ± 0.107 |
| BayesDirect | 0.244 ± 0.110 | 0.286 ± 0.109 | 0.337 ± 0.108 | 0.433 ± 0.198 | 0.469 ± 0.295 |

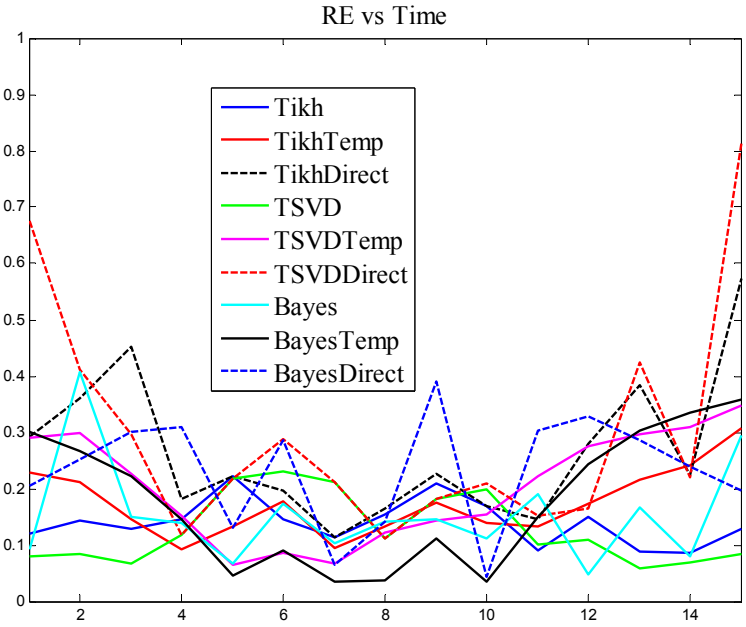


Figure 4.6 : The relative error vs. time graph of the methods that are used the in the simulation

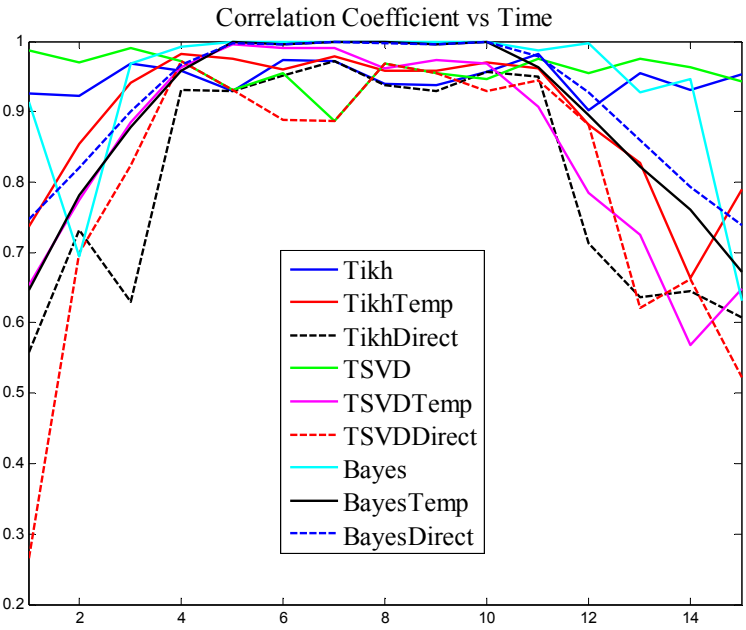


Figure 4.7 : The Correlation Coefficient over time instants of the methods

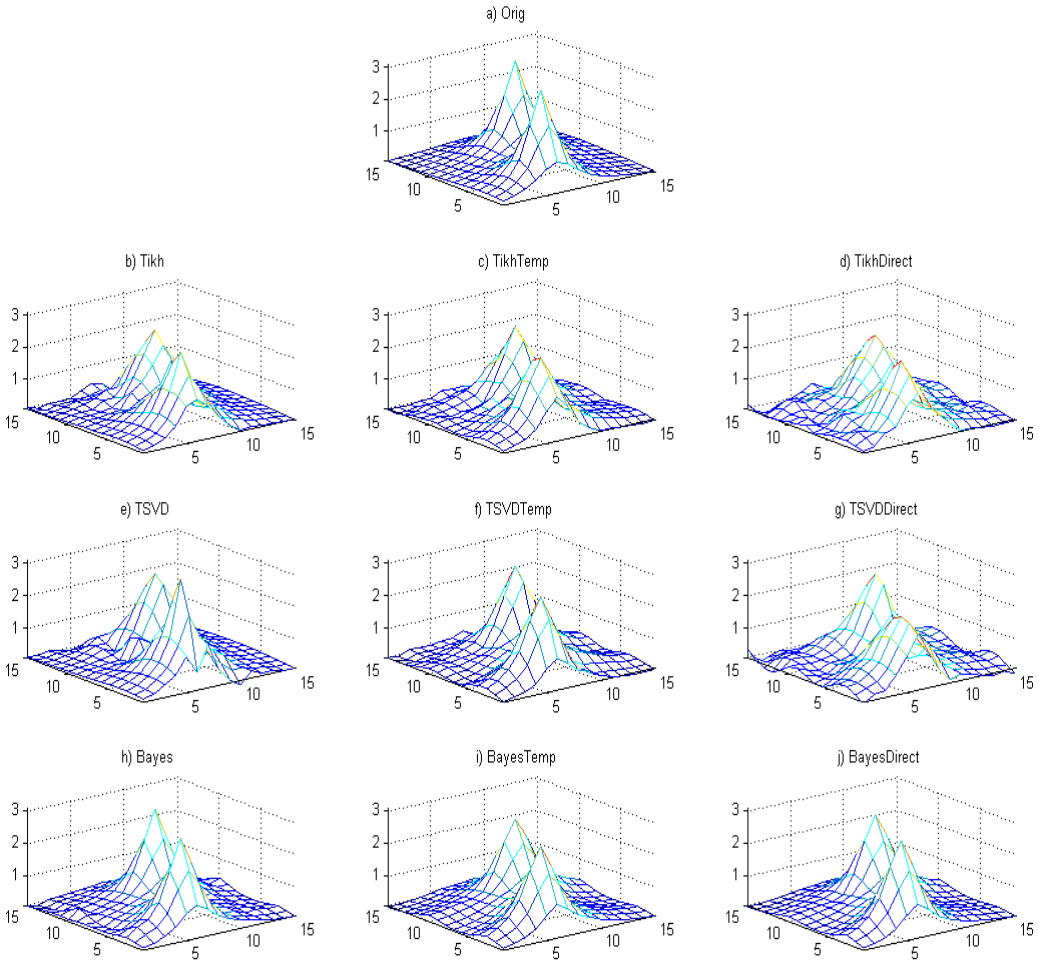


Figure 4.8 : The 3D visualizations of the data and its estimations. a) the original data b) Tikhonov solution c) Tikhonov solution after Temporal whitening d) Direct Tikhonov solution e) TSVD solution f) TSVD solution after temporal whiting g) Direct TSVD solution h) Bayes MAP solution i) Bayes MAP after temporal whitening j) Direct Bayes solution .

It can be easily seen in Figure 4.8 Bayes methods, especially BayesDirect, method have more resemblance to the original signal distribution. In Tikhonov and TSVD solutions, the peaks are not sharp. The temporal whitening affected the region around the peaks, but effect on the sharpness of the peaks is little. In Figure 4.6 and Figure 4.7, the performances are similar.

In table 4.1, noise performances of the methods reduce with decreasing SNR. Standard Bayes solution has an interesting variation. In the 30 dB SNR noise level, it has more efficient results than Tikhonov and TSVD solutions, however; RE values at 2.4 SNR noise level is mostly larger than the others are.

### 4.4.2 Experiment 2 with Data 2

In this example, we use the data described in section 4.1.1 – b) [53]. The error performances of the methods with respect to relative errors and correlation coefficients are given in figure 4.9 and figure 4.10, respectively. The average values of RE at different noise levels is given in table 4.2. The 3D plots of the methods are given in figure 4.11.

Table 4.2 : The average value and standard deviation of the relative error

| SNR (dB) | 30 | 18 | 9.6 | 4.8 | 2.4 |
|---|---|---|---|---|---|
| Tikh | 0.228 ± 0.040 | 0.312 ± 0.054 | 0.390 ± 0.075 | 0.423 ± 0.079 | 0.468 ± 0.088 |
| TikhTemp | 0.197 ± 0.021 | 0.255 ± 0.039 | 0.351 ± 0.055 | 0.366 ± 0.070 | 0.403 ± 0.084 |
| TikhDirect | 0.245 ± 0.040 | 0.330 ± 0.047 | 0.407 ± 0.082 | 0.444 ± 0.089 | 0.497 ± 0.079 |
| TSVD | 0.235 ± 0.027 | 0.327 ± 0.041 | 0.396 ± 0.049 | 0.464 ± 0.053 | 0.506 ± 0.066 |
| TSVDTemp | 0.202 ± 0.021 | 0.269 ± 0.044 | 0.340 ± 0.068 | 0.387 ± 0.052 | 0.410 ± 0.108 |
| TSVDDirect | 0.255 ± 0.021 | 0.355 ± 0.062 | 0.424 ± 0.072 | 0.506 ± 0.064 | 0.548 ± 0.167 |
| Bayes | 0.123 ± 0.030 | 0.123 ± 0.035 | 0.247 ± 0.079 | 0.299 ± 0.088 | 0.353 ± 0.158 |
| BayesTemp | 0.123 ± 0.034 | 0.187 ± 0.067 | 0.277 ± 0.113 | 0.309 ± 0.118 | 0.378 ± 0.137 |
| BayesDirect | 0.116 ± 0.033 | 0.136 ± 0.109 | 0.169 ± 0.053 | 0.207 ± 0.165 | 0.276 ± 0.163 |

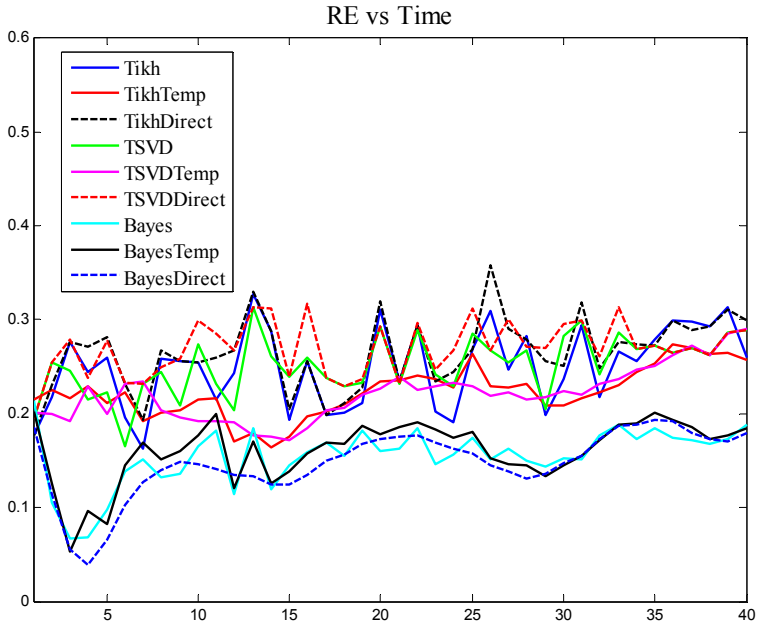


Figure 4.9 : The relative error vs. time graph for the methods

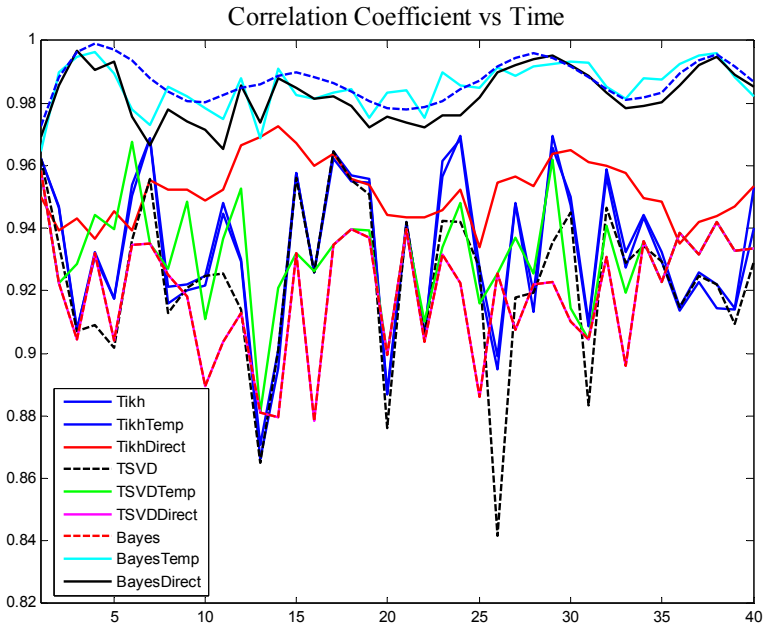


Figure 4.10 : The Correlation Coefficient across time instants

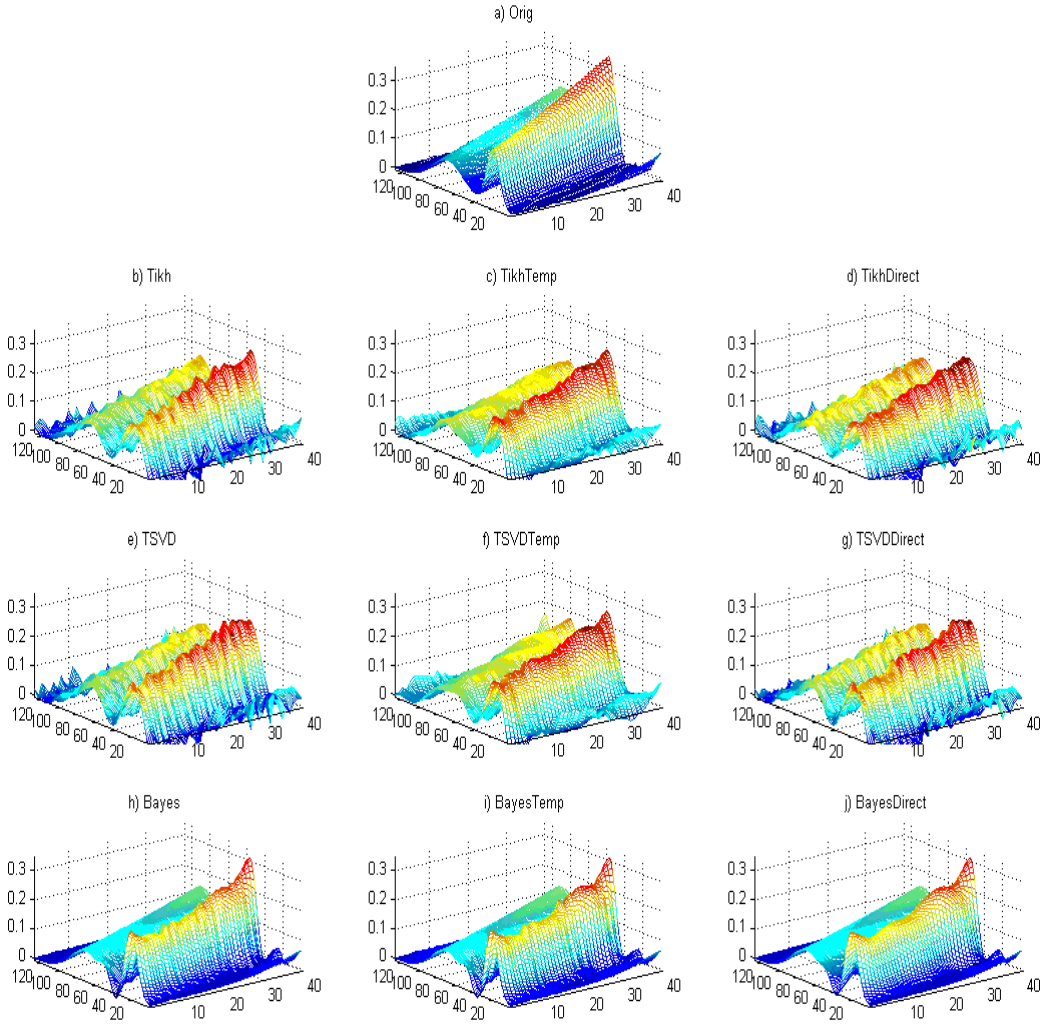


Figure 4.11 : The 3D visualizations of the data and its estimations. a) the original data b) Tikhonov solution c) Tikhonov solution after Temporal whitening d) Direct Tikhonov solution e) TSVD solution f) TSVD solution after temporal whiting g) Direct TSVD solution h) Bayes MAP solution i) Bayes MAP after temporal whitening j) Direct Bayes solution

The BayesDirect method gives the best result. The Bayesian solution has better error performance than TSVD and Tikhonov solutions. After the temporal whitening, the fluctuations on the peaks are reduced. The direct solution has an improvement on Bayesian MAP, but in Tikhonov and TSVD, the resolution decreases.

### 4.4.3 Simulated Torso Potentials

In this experiment, we used the simulated torso potential measurements as explained in section 4.1.2. In this experiment, we could not apply the direct solution of Bayesian estimation (BayesDirect) since the $C_X$ in (3.33) has a dimension of 53410×53410 and also inversion of the matrix in (3.35) is difficult due to the its large dimension (84039×84039). Therefore, for only registering the matrix we have to need a machine with at least 53 GB RAM. The machine that we used has 4 GB RAM. As a result, we solved the inverse problem with these data using the remaining six methods.

In Bayes MAP solution, we used the column sequential approach. In this method, the covariance matrix was computed using autocorrelation method and we use same covariance matrices for all time instants. In the BayesTemp method, we used the separability condition [2]. The covariance matrix $C_X$ was not computed directly due to high dimensions (53410×53410). Instead of direct computation, we calculated it by dividing into blocks. Since we solved the problem sequentially, it required only the diagonal blocks. After temporal whitening, the covariance matrix of transformed parameter $C_{XZ}$ was calculated as a block matrix using (3.61).

Table 4.3 : The average and standard deviation values of RE and CC

| Methods | Average RE ± std | Average CC ± std |
|---|---|---|
| **Tikh** | 0.513 ± 0.182 | 0.794 ± 0.200 |
| **TikhTemp** | 0.500 ± 00218 | 0.816 ± 0.208 |
| **TSVD** | 0.518 ± 0187 | 0.791 ± 0.206 |
| **TSVDTemp** | 0.508 ± 0.256 | 0.818 ± 0.209 |
| **Bayes** | 0.344 ± 0.369 | 0.894 ± 0.209 |
| **BayesTemp** | 0.326 ± 0.348 | 0.890 ± 0.207 |

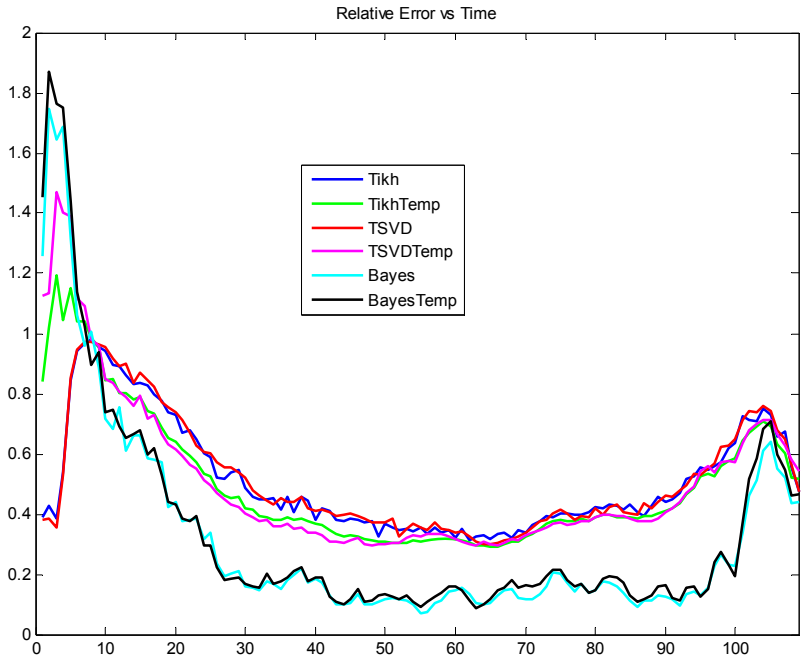


Figure 4.12 : The relative error across time graph of the method

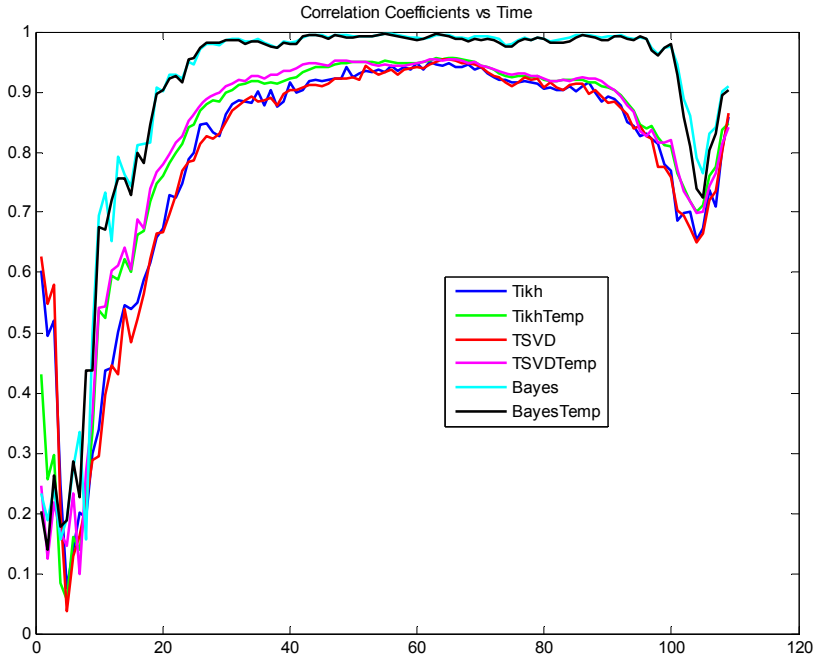


Figure 4.13 : The CC vs. time graph of the methods

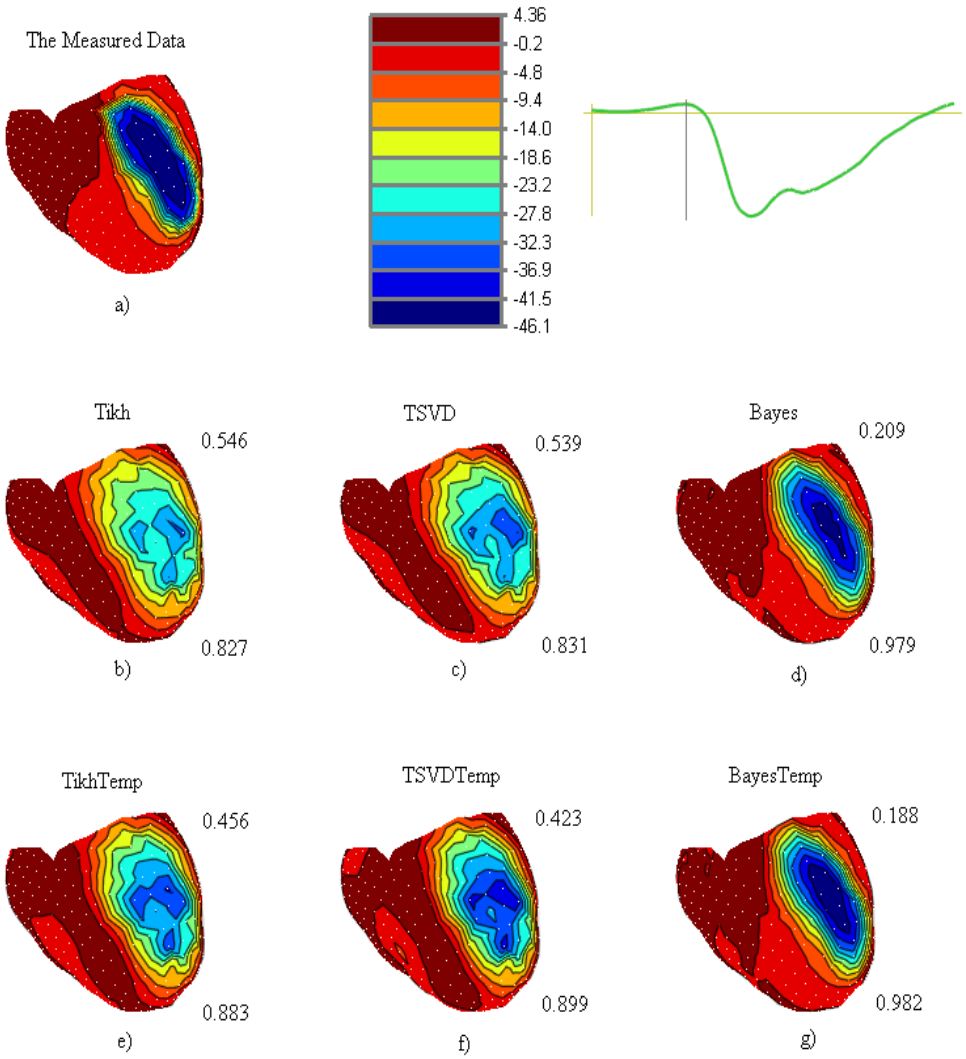


Figure 4.14 : The map3d visualization of data and its estimations at 29 ms. The value at upper right side represents the RE value and the value at lower left represents the CC value at that time. a) The measured data b) Tikhonov Solution c) TSVD Solution d) Bayes MAP solution g) Bayes solution after temporal whitening e) Tikhonov after Temporal Whitening f) TSVD after Temporal Whitening g) Bayes solution after Temporal Whitening

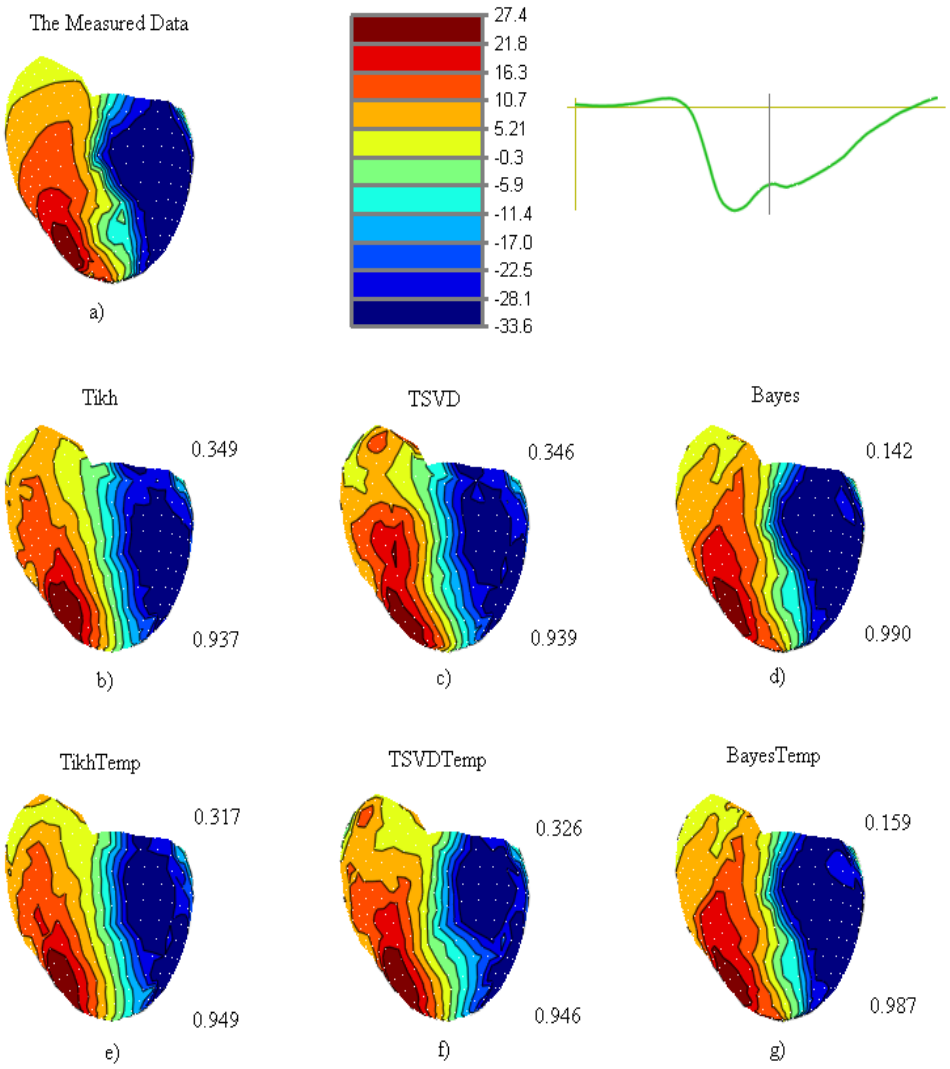


Figure 4.15 : The map3d visualization of data and its estimations at 59 ms. The value at upper right side represents the RE value and the value at lower left represents the CC value at that time. a) The measured data b) Tikhonov Solution c) TSVD Solution d) Bayes MAP solution g) Bayes solution after temporal whitening e) Tikhonov after Temporal Whitening f) TSVD after Temporal Whitening g) Bayes solution after Temporal Whitening

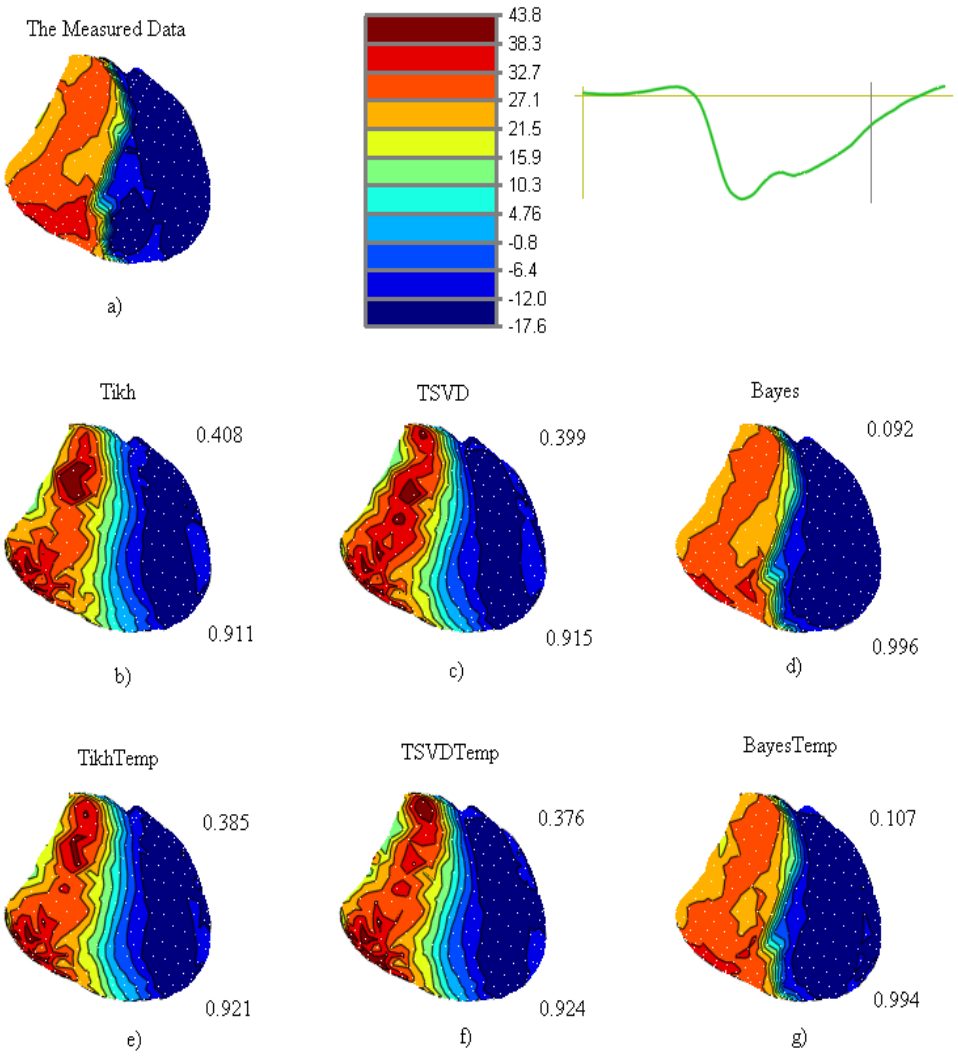


Figure 4.16: The map3d visualization of data and its estimations at 86 ms. The value at upper right side represents the RE value and the value at lower left represents the CC value at that time. a) The measured data b) Tikhonov Solution c) TSVD Solution d) Bayes MAP solution g) Bayes solution after temporal whitening e) Tikhonov after Temporal Whitening f) TSVD after Temporal Whitening g) Bayes solution after Temporal Whitening

The error performance at 30 dB noise level is given in figure 4.12 and figure 4.13 and table 4.3. Figures 4.12, 4.13 and 4.14 give the 3D illustrations of the

solution at 29, 59 and 86 ms after the initial stimulation, respectively. In these illustrations, the red regions represent the parts of the epicardium not activated yet (positive) and the blue regions have already been activated (negative).

The performances of Bayes solutions with respect to RE and CC values are better than the performances of the other methods. The Tikhonov and TSVD solutions reflect the wavefront propagation pattern of the true epicardial potential maps in general; however, they cannot follow the wavefront on the epicardium as well as the Bayesian solutions do.

### 4.5 Discussion

In the previous part, we presented the simulation results of the methods explained in the thesis using three different data sets. In this part, we discuss the results over the 3D illustrations and error performance measures. For error performance, we have examined the relative errors and the correlation coefficients of the estimations.

In the first two examples, we use all of the methods. However, in the last simulation, we cannot apply the direct solution method to the data due to high dimensionality of the problem. Hence, we only use the methods that employ the column sequential and the temporal whitening approaches for the simulated torso potential example.

If we assess the results as a whole, the Bayesian MAP solutions (Bayes, BayesDirect and BayesTemp) have better error performances and results than those of the Tikhonov and TSVD solutions, since we have known from the

theory that Bayes MAP is a statistical estimation method that uses a known prior pdf. This allows us to gain more information about the unknown, so it supplies less perturbation in the solution. In addition, we use the covariance matrix $C_X$ in the formulation of the Bayesian estimation. As mentioned before, the covariance matrix contains temporal and spatial information about the unknown. It supplies more information about the characteristics of the solution. In this study, we formed this covariance matrix from the measurements. This covariance matrix is very close to the real covariance matrix. On the other hand, in the Tikhonov regularization we obtained the information only from the constraint imposed to the minimization problem to solve the ill-conditioned matrix equation. In TSVD, we truncate the decomposition process by throwing out the smaller singular values, thus the solutions were distorted due to this truncation.

Especially, the BayesDirect method gives the best results in the first two examples. In the direct method, we use a full covariance matrix and then solve the augmented problem directly.

When we examine the performance of each approach at different noise levels (table 4.1, table 4.2 and table 4.3) using the synthetic data, we observe that the performance of the methods reduce with low SNR value. The Tikhonov and TSVD solutions are more robust than the Bayesian solutions.

As we examine the effects of temporal whitening on the methods, it can be easily seen that the improvements on TSVD and Tikhonov solutions after temporal whitening is more detectable than in the Bayes MAP solution. This is because the first two methods have more perturbation than the other one, and we know that temporal whitening is an equivalent process to apply a smoothing filter. Another reason is the usage of $C_X$ that is obtained from the true parameter

matrix, **X**, in Bayes estimation, and the Bayes solution (without temporal whitening) already produces very successful reconstructions. Adding temporal correlations does not cause a serious change on the solution.

In the simulated torso potential example, Tikhonov and TSVD solutions cannot follow the wavefront on the epicardium as well as Bayesian solutions due to smoothing effects of Tikhonov regularization and truncation effects of TSVD.

As a summary, imposing temporal correlations to the solutions provides improvements on the solutions, especially to the Tikhonov regularization and the TSVD results. These improvements are more obvious for the first two simulations. The Bayesian solutions are much better than the others due to usage of $C_X$ created from the measurements itself.

# CHAPTER 5

## CONCLUSIONS AND FUTURE WORK

A detailed study has been undertaken to evaluate the performance of spatial and spatio-temporal regularization methods and approaches in inverse electrocardiography. We used three different essential methods. These methods are Tikhonov Regularization, TSVD and Bayesian MAP estimation. We solved the inverse problem using these three methods with and without temporal correlation.

The easiest and fastest approach is to solve the system independently for each time instant. This solution approach requires no temporal correlation assumption. In the temporal correlation assumption, we have two alternatives. We can solve the augmented system in (3.33) at once or we can use the column sequential method after the system is decorrelated by applying a temporal whitening filter.

We use the separability condition for Bayesian MAP estimation. With this condition, the covariance matrix can be represented separately in terms of its spatial and temporal covariance matrices. This allows us to use the spatial and temporal constraints simultaneously. Applying temporal whitening with this condition, the transformed covariance matrix can be represented in terms of the original covariance matrix.

In order to compare the performances of these methods, we used three simulated data sets. In first two experiments, we used synthetic data. In the last one, we used simulated torso potentials obtained from true epicardial potentials measured from a canine heart. We investigated the error performances with respect to RE and CC. In addition, we analyzed the 3D distributions of the results.

Based on the results in this study, following conclusions were drawn.

1) The Bayes approaches have better results than the direct regularization methods (TSVD and Tikhonov regularization), especially when the covariance matrix is obtained from the true epicardial potential distributions.

2) The Temporal whitening procedure has more effects on the TSVD and Tikhonov regularization.

3) Using separability condition, we can obtain more information about the characteristics of the unknown. In temporal whitening procedure, it accelerates the process.

4) Direct solution is the best method although it is very slow due to complexity of the problem. Therefore, it could not be applied directly to large problems such as epicardial simulation, because it requires a large memory in the computer.

## 5.1 The Future Work

In this study, we could not apply BayesDirect method to epicardial data due to high dimensionality of the problem. One possible way to overcome this difficulty is to use a suitable iterative method such as block Cholesky factorization. Another alternative is to use parallel processing. We have two alternatives for that purpose: in the first one, we can form a suitable cluster in the local area and the process can be distributed on the elements of the cluster. The other one is to solve the problem by the means of grid that is a type of distributed computing. A grid composed of a cluster of networked, loosely coupled computers, acting in order to perform very large tasks.

Another possibility for further studies is to define the spatio-temporal covariance matrix $C_X$ without the use of true unknown epicardial distribution. One way to do this is to use training sets.

# REFERENCES


[1] Gulrajani R.M, "*The forward and inverse problems of Electrocardiography*" IEEE Engineering in Medicine and Biology, vol. 17, pp. 84 – 101, Sep-Oct. 1998

[2] Greensite F., "*A new treatment of the inverse problem of multivariate analysis*" Inverse Problems, vol. 18, pp. 363–379, 2002

[3] Morgan C.E., "*Electro-Physiology and* Therapeutics" Williams, Wood, New York 1868

[4] Krueger J., "*Beschichte der Erde*" Lubetvatbischen Buchhandlung, Helmstädt, 1746

[5] Galvani L., "De viribus electricitatis in motu musculari. Commentarius. *De Bononiesi Scientarium et Ertium Instituto atque Academia Commentarii*" 7: 363-418 (Commentary on the effects of electricity on muscular motion) Burndy Library edition, 1953, Norwalk, Conn.

[6] Malmivuo J., Plonsey R., "*Bioelectromagnetism - Principles and Applications of Bioelectric and Biomagnetic Fields*", Oxford University Press, New York, 1995

[7] Matteuci C., "Deuxième mémoire sur le courant électrique propre de la grenouille et sur celui des animaux à sang chaud" Ann. Chim. Phys. *(3ème serie,)* 6: 301-39

[8] DuBois-Reymond E., "*Untersuchungen über tierische Elektizität*" Bd. I u. II Berlin, Reimer, 1848

[9] Waller A.D. "*A demonstration on man electromotive changes accompanying the heart's beat*", J. Pysiol. 8:229-34, 1887

[10] Lippmann G., "*Relations entre les phenomenos electriques et capillaries*", Ann. Chim. Phys. Ser. 5, 5, 494 1875

[11] Einthoven W., Fahr G. and de Waart A., "*Über die Richtung und die Manifeste Grösse der Potentialschwankungen im mennschlichen Herzen und über den Einfluss der Herzlage auf die form des Elektrokardiogramms*" Pflüger Arch. ges. Physiol. 150: 275-31, 1913

[12] Zywietz, C. "*A brief history of bioelectricity and electricity generated by heart*", http://www.openecg.net/Tutorials/A_Brief_History_of_Electrocardiography.pdf

[13] Pullan A. J., Buist M. L., and Cheng L. K. " *Mathematically modeling of the electrical activity of the heart: From cell to body surface and back again*" Worl Scientific, New Jersey, 2005

[14] Gulrajani R.M., "*Bioelectricity and Biomagnetism*" John Wiley & Sons, Inc.; New York: 1998

[15] Plonsey R. "Bioelectric Phenomena", McGraw-Hill, New York, 1969

[16] Wikimedia Foundation, Inc, "*Action potential*", http://en.wikipedia.org/wiki/Action_potential, September 2008

[17] Dorland's Medical Dictionary for Health Consumers, "*definition of electrogram*", http://medical-dictionary.thefreedictionary.com/electrogram, 2007

[18] Wilson F.N., Johnston F.D., Macleod A.G., and Barker P.S., "*Electrocardiograms that represent the potential variations of a single electrode*" Am. Heart J. 9: 447-71, 1934

[19] Goldberger E., "*The aVL, aVR, and aVF leads; A simplification of standard lead electrocardiography*" Am. Heart J. 24: 378-96, 1942

[20] Wilson F.N., Johnston F.D., Rosenbaum F.F., Erlanger H., Kossmann C.E., Hecht H., Cotrim N., Menezes de Olivieira R., Scarsi R., and Barker P.S., "*The precordial electrocardiogram*" Am. Heart J. 27: 19-85, 1944

[21] Medvegy M., Duray G., Pinter A., and Preda I., "*Body surface potential mapping: historical* background, present possibilities, diagnostic challenges" Ann. of Noninvasive Electrocardiology, Vol. 7 No. 2: 139-151, 2002

[22] http://biomed.tkk.fi/OLD/annual/96_97/node23.html

[23] Yamashita Y., "*Theoretical studies on the inverse problem in electrocardiography and the uniqueness of the solution*" IEEE Trans. Biomed. Eng. 29; 719-725, 1982

[24] Arthur R.M., "*Quadrupole components of the human surface electrocardiogram*" Ann. Heart J. 83: 663-667, 1972

[25] Arthur R.M., Geselowitz D.B., Briller S.A., Trost R.F. "*The path of the electrical center of the human heart determined from surface electrocardiograms*" J. Electrocardiol. 4:(1) 29-33, 1971

[26] Ralston A., and Rabinowitz P., "*A first course on numerical analysis*" McGraw-Hill, New York, 1978

[27] Fischmann E.J., Barber M.R. "*'Aimed' electrocardiography. Model studies, using a heart consisting of 6 electrically isolated areas*" Am. Heart J. 65:(5) 628-37, 1963

[28] Selvester R.H., Collier C.R., Pearson R.B. "*Analog computer model of the vectorcardiogram*" Circulation 31:(1) 45-53, 1965

[29] He B., Cohen R.J. "*Inverse Multiple Dipole Solutions from Body Surface Laplacian Maps*" In: Proc. 14th Ann. Int. Conf. IEEE Eng. Med. Biol. Soc IEEE Press, New York, pp 2011-2012, 1992

[30] MacLeod R. S., Brooks D. H., "*Recent progress in inverse problems in electrocardiography*" IEEE Eng. Med. Biol. 17: (1) 73-83, 1998

[31] Cuppen J. J. M., Van Oosterom A, "*Model studies with the inversely calculated isochrones of ventricular depolarization*" IEEE Trans. Biomed. Eng. BME-3 1:652-659, 1984

[32] Huiskamp G. J., Van Oosterom A, "*The depolarization sequence of the human heart surface computed from measured body surface potentials*" IEEE Trans. Biomed. Eng. BME-35: 1047-1059

[33] Tikhonov A.N. and Arsenin V.Y., "*Solution of Ill-posed Problems*" V. H. Winston and Sons (distributed by Wiley, New York), Washington, DC, 1977

[34] Morozov M.A., "*Methods for solving incorrectly posed problems*" Springer-Verlag, New York, pp44-47, 1984

[35] Wahba G., "Practical approximate solutions to linear operator equations when the data are noisy" SIAM J. Num. Anal. 14: 651-667, 1977

[36] Golub G.H., Heat M., Wahba G., "*Generalized cross-validation as a method for choosing a good ridge parameter*" Technometrics 21:215-223, 1979

[37] Colli Franzone P., Guerri L., Taccardi B., Viganotti C., "*Finite element approximation of regularized solutions of the inverse potential problem of electrocardiography and applications to experimental dat*" Calcolo, 22:91-186, 1985

[38] Twomey S., "*On the numerica solution of Fredholm integral equations of the first kind by the inversion of the linear sytem produced by quadrature*" JACM, 10:97-101, 1963

[39] Oster H., Rudy Y., "*Regional Regularization of the elctrocardiographic inverse problem: a modelstudy using spherical geometry*" IEEE Trans. Biomed. Eng. 44:188-199, 1997

[40] Barr R.C., Spach M.S., "*Inverse calculation of QRS-T potentials from body surface potential distributions for normal and ectopic beats in the intact dog*" Circ. Res. 42: 661-675, 1978

[41] Oster H., Rudy Y., "*The use of temporal information in the regularization of the inverse electrocardiography*" IEEE Trans. Biomed. Eng. 39:65-75, 1992

[42] Brooks D.H., Maratos G.M., Ahmad G., MacLeod R.S., "*The augmented inverse problem of electrocardiography: combined time and space regularization*" In: Proc. 16th Ann. Int. Conf. IEEE Eng. Med. Biol. Soc., IEEE Press, New York, pp 773-774, 1993

[43] Brooks D.H., Ahmad G., MacLeod R.S., "*Multiply constrained inverse electrocardiography: combined temporal, multiple spatial, and interative regularization*" In: Proc. 16th Ann. Int. Conf. IEEE Eng. Med. Biol. Soc., IEEE Press, New York, pp 773-774, 1993

[44] Zhang Y., Ghodrati A., Brooks D.H., "*An analytical comparison of three spatio-temporal regularization methods for dynamic linear inverse problems in a common statistical framework*" Inverse Problems, vol. 21, pp. 357-382, 2005

[45] Greensite F., "*The temporal behaviour in bioelectromagnetic source imaging problems*" IEE Trans. Biomed. Eng. 50:1152-9, 2003

[46] Joly D., Goussard Y. and Savard P. "*Time-recursive solution to the inverse problem of electrocardiography: a model-based approach*" Proc. 15th Ann. IEEE-EMBS Conf. pp 767–8, 1993

[47] El-Jakl J., Champagnat F. and Goussard Y. "*Time-space regularization of the inverse problem of electrocardiography*" Proc. 17th Ann. IEEE-EMBS Conf. pp 213–4, 1995

[48] Rauch H., Tung F. and Striebel C., "*Maximum likelihood estimates of linear dynamic systems*" AIAA J. 3:1445, 1965

[49] Brooks D.H.., Ghandi F.A., Macleod S., "*Inverse Electrocardiography by Simultaneous Imposition of Multiple Constraints*" IEEE Transactions on Biomedical Engineering, vol. 46, no. 1, January 1999

[50] Hadamard J., "*Lecture on Cauchy's Problem on Linear Partial Differential Equations*" Yale University Press, New Haven, CT, 1923

[51] Hansen P. C., "*Rank-Deficient and Discrete Ill-Posed Problems: Numerical Aspects of Linear Inversion*" SIAM, 1998

[52] Kay S.M., "*Fundamentals of Statistical Signal Processing: Estimation Theory*" Englewood Cliffs, NJ: Prentice-Hall, 1993

[53] Serinağaoğlu Y. "*Bayesian Solutions and Performance Analysis in Bioelectric Inverse Problems*" IEEE Transactions on Biomedical Engineering, vol. 52, no. 6, June 2005

[54] He R., Rao H., Liu S., Yan W., Narayana P.A., and Brauer H. "*The method of maximum mutual information for biomedical electromagnetic inverse problems*" IEEE, Trans. on Magnetics 36: 1741-1744, July 2000

[55] Aster R., Borchers B. and Thurber T., "*Parameter Estimation and Inverse Problems*" Academic Press, 2004

[56] MacLeod R. S. and Johnson C. R., "Map3d: Interactive scientific visualization for bioengineering data," Proc. Eng. Med. Biol. Soc. 15th Ann. Int. Conf., vol. 44, pp. 196–208, 1997

[57] R.S. Macleod, R.L. Lux, and B. Taccardi, "*A possible mechanism for electrocardiographically silent changes in cardiac repolarization*" J. Electrocardiol., Vol. 30, Suppl.: 114-121, 1997

# APPENDICES

## APPENDIX A

## KRONECKER PRODUCT

The Kronecker product is defined for two arbitrary matrices on any ring. For the matrices; $\mathbf{A} \in R^{m \times n}$ and $\mathbf{B} \in R^{p \times q}$ the Kroneceker product is:

$$\mathbf{A} \otimes \mathbf{B} = \begin{bmatrix} a_{11}\mathbf{B} & \cdots & a_{1n}\mathbf{B} \\ \vdots & & \vdots \\ a_{m1}\mathbf{B} & \cdots & a_{\mathbf{mn}}\mathbf{B} \end{bmatrix} \tag{A1}$$

The Kronecker product is a special case of Tensor product.

**A1 Ptoperties of The Kronecker Product**

Let **A**,**B**,**C**,**D** are the real valued matrices and α is a real constant.

$$\begin{aligned} \mathbf{A} \otimes (\alpha \mathbf{B}) &= \alpha(\mathbf{A} \otimes \mathbf{B}) \\ (\alpha \mathbf{A}) \otimes \mathbf{B} &= \alpha(\mathbf{A} \otimes \mathbf{B}) \end{aligned} \tag{A2}$$

$$\begin{aligned} (\mathbf{A} + \mathbf{B}) \otimes \mathbf{C} &= (\mathbf{A} \otimes \mathbf{C}) + (\mathbf{B} \otimes \mathbf{C}) \\ \mathbf{A} \otimes (\mathbf{B} + \mathbf{C}) &= (\mathbf{A} \otimes \mathbf{B}) + (\mathbf{A} \otimes \mathbf{C}) \end{aligned} \tag{A3}$$

$$(\mathbf{A} \otimes \mathbf{B}) \otimes \mathbf{C} = \mathbf{A} \otimes (\mathbf{B} \otimes \mathbf{C}) \tag{A4}$$

$$(\mathbf{A} \otimes \mathbf{B}) \neq (\mathbf{B} \otimes \mathbf{A}) \tag{A5}$$

$$(\mathbf{A} \oplus \mathbf{B})^T = \mathbf{A}^T \otimes \mathbf{B}^T \tag{A6}$$

$$(\mathbf{A} \otimes \mathbf{B})(\mathbf{C} \otimes \mathbf{D}) = (\mathbf{AC} \otimes \mathbf{BD}) \tag{A7}$$

**A** & **B** are square and full rank matrices

$$(\mathbf{A} \otimes \mathbf{B})^{-1} = \mathbf{A}^{-1} \otimes \mathbf{B}^{-1} \ \mathbf{B} \tag{A8}$$

Let $\mathbf{A} \in R^{n \times n} \mathbf{B} \in R^{m \times m}$

$$\det(\mathbf{A}_{n \times n} \otimes \mathbf{B}_{m \times m}) = \det(\mathbf{A})^m \det(\mathbf{B})^n \tag{A9}$$

# APPENDIX B

# THE FROBENIUS NORM AND TRACE

The Frobenius norm is a $L^2$ norm that defined for matrices. It sometimes is called Euclidean norm or Hilbert-Schmidt norm. The Frobenius norm of a matrix $\mathbf{A} \in R^{m \times n}$ is defined as:

$$\|\mathbf{A}\|_F^2 = \sum_{i=1}^{m}\sum_{j=1}^{n} |a_{ij}|^2 = \text{trace}(A^T A) = \sum_{i=1}^{\min(m,n)} \sigma_i \qquad \text{(B1)}$$

where $\sigma_i$ is the singular value.

We use the second definition that contains the "trace" operation. The "trace" operation is defined as the sum of the elements at the main diagonal for an nxn matrix A.

$$trace(\mathbf{A}) = \sum_{i=1}^{n} a_{ii}$$

**B1. Properties of Trace**

Let **A** and **B** are real valued matrix and α is a scalar:

$$\text{trace}(\mathbf{A}+\mathbf{B}) = \text{trace}(\mathbf{A}) + \text{trace}(\mathbf{B}) \qquad \text{(B1)}$$

$$\text{trace}(\alpha\mathbf{A})=\alpha.\text{trace}(\mathbf{A}) \tag{B2}$$

$$\text{trace}(\mathbf{A}^T)=\text{trace}(\mathbf{A}) \tag{B3}$$

**A** & **B** such that **AB** is a square matrix

$$\text{trace}(\mathbf{AB})=\text{trace}(\mathbf{BA}) \tag{B4}$$

$$\text{trace}(\mathbf{A})=\text{trace}(\mathbf{B}^{-1}\mathbf{AB}) \tag{B5}$$

$$\text{trace}(\mathbf{A}^T\mathbf{A})=\text{trace}(\mathbf{A}\mathbf{A}^T) \tag{B6}$$

# APPENDIX C

# THE ORTHOGONAL MATRIX

In Linear Algebra, real orthogonal matrix is a square matrix whose transpose is the inverse matrix of itself. In mathematical description:

$$\mathbf{A}^T\mathbf{A} = \mathbf{A}\mathbf{A}^T = \mathbf{I} \tag{C1}$$

Therefore, orthogonal matrices are also unitary matrices.